Title

Seasonal differences in the photochemistry of the South Pacific: A comparison of observations and model results from PEM-Tropics A and B

Journal

Journal of Geophysical Research Atmospheres, 106(D23)

ISSN

0148-0227

Authors

Olson, JR
Crawford, JH
Davis, DD
et al.

Publication Date

2001-12-16

DOI

10.1029/2001JD900077

JOURNAL OF GEOPHYSICAL RESEARCH, VOL. 106, NO. D23, PAGES 32,749–32,766, DECEMBER 16, 2001

Seasonal differences in the photochemistry of the South Pacific: A comparison of observations and model results from PEM-Tropics A and B

J. R. Olson,[1] J. H. Crawford,[1] D. D. Davis,[2] G. Chen,[2] M. A. Avery,[1] J. D. W. Barrick,[1] G. W. Sachse,[1] S. A. Vay,[1] S. T. Sandholm,[2] D. Tan,[3,4] W. H. Brune,[3] I. C. Faloona,[3] B. G. Heikes,[5] R. E. Shetter,[6] B. L. Lefer,[6] H. B. Singh,[7] R. W. Talbot,[8] and D. R. Blake[9]

Abstract. A time-dependent photochemical box model is used to examine the photochemistry of the equatorial and southern subtropical Pacific troposphere with aircraft data obtained during two distinct seasons: the Pacific Exploratory Mission-Tropics A (PEM-Tropics A) field campaign in September and October of 1996 and the Pacific Exploratory Mission-Tropics B (PEM-Tropics B) campaign in March and April of 1999. Model-predicted values were compared to observations for selected species (e.g., NO_2, OH, HO_2) with generally good agreement. Predicted values of HO_2 were larger than those observed in the upper troposphere, in contrast to previous studies which show a general underprediction of HO_2 at upper altitudes. Some characteristics of the budgets of HO_x, NO_x, and peroxides are discussed. The integrated net tendency for O_3 is negative over the remote Pacific during both seasons, with gross formation equal to no more than half of the gross destruction. This suggests that a continual supply of O_3 into the Pacific region throughout the year must exist in order to maintain O_3 levels. Integrated net tendencies for equatorial O_3 showed a seasonality, with a net loss of 1.06×10^{11} molecules cm^{-2} s^{-1} during PEM-Tropics B (March) increasing by 50% to 1.60×10^{11} molecules cm^{-2} s^{-1} during PEM-Tropics A (September). The seasonality over the southern subtropical Pacific was somewhat lower, with losses of 1.21×10^{11} molecules cm^{-2} s^{-1} during PEM-Tropics B (March) increasing by 25% to 1.51×10^{11} molecules cm^{-2} s^{-1} during PEM-Tropics A (September). While the larger net losses during PEM-Tropics A were primarily driven by higher concentrations of O_3, the ability of the subtropical atmosphere to destroy O_3 was ~30% less effective during the PEM-Tropics A (September) campaign due to a drier atmosphere and higher overhead O_3 column amounts.

1. Introduction

A major focus in tropospheric chemistry in recent years has been to advance our understanding of processes that impact tropospheric ozone (O_3) from local to global scales. High concentrations of O_3 near the earth's surface have deleterious impacts on human health [*Horvath and McKee*, 1994] and on vegetation and crop yields [e.g., *Chameides et al.*, 1994], and O_3 is an important species in consideration of the Earth's energy budget [*Ramanathan et al.*, 1976; *Ramanathan and Dickenson*, 1979; *Fishman et al.*, 1979]. In addition, the abundance and distribution of O_3 throughout the troposphere governs the oxidative capacity of the troposphere. Photodissociation of O_3 in the presence of water vapor initiates the formation of the hydroxyl (OH) radical, which is responsible for the chemical removal of atmospheric pollutants. Most oxidation of long-lived gases such as CO and CH_4 occurs at tropical latitudes, where conditions for OH formation are favorable because of the moist atmosphere and abundant sunlight.

Global sources of tropospheric O_3 include transport from the stratosphere and photochemical production within the troposphere [*Danielson*, 1968; *Crutzen*, 1973; *Chameides and Walker*, 1973]. Quantification of these two sources has been a major goal of many studies [e.g., *Chatfield and Harrison*, 1976; *Fabian and Pruchniewicz*, 1977; *Liu et al.*, 1980; *Gidel and Shapiro*, 1980; *Logan*, 1985; *Roelofs et al.*, 1997; *Wang et al.*, 1998; *Lelieveld and Dentener*, 2000]. Tropospheric photochemical O_3 production occurs via oxidation of CO, CH_4,

[1]Atmospheric Sciences Competency, NASA Langley Research Center, Hampton, Virginia.
[2]School of Earth and Atmospheric Sciences, Georgia Institute of Technology, Atlanta, Georgia.
[3]Department of Meteorology, Pennsylvania State University, University Park, Pennsylvania.
[4]Currently at School of Earth and Atmospheric Sciences, Georgia Institute of Technology, Atlanta, Georgia.
[5]Center for Atmospheric Chemistry Studies, Graduate School of Oceanography, University of Rhode Island, Narragansett, Rhode Island.
[6]Atmospheric Chemistry Division, National Center for Atmospheric Research, Boulder, Colorado.
[7]Chemistry and Dynamics Branch, NASA Ames Research Center, Moffett Field, California.
[8]CSRC/EOS, University of New Hampshire, Durham, New Hampshire.
[9]Department of Chemistry, University of California-Irvine, Irvine, California.

Paper number 2001JD900077.
0148-0227/01/2001JD900077$09.00

or nonmethane hydrocarbons (NMHC) in the presence of nitrogen oxides (NO_x = NO + NO_2) and solar radiation. The global distribution of tropospheric NO_x, which is the critical limiting precursor for O_3 production, is highly variable and is dependent on local photochemical loss and cycling processes as well as on the magnitude of various sources which include transport from the stratosphere, natural emissions (lightning, soils, biomass burning) and anthropogenic emissions (industrial, aircraft, ships) [*Hameed et al.*, 1981; *Liu et al.*, 1980; *Logan*, 1983; *Kasibhatla et al.*, 1991; *Penner et al.*, 1991; *Kasibhatla et al.*, 1993; *Kasibhatla*, 1993; *Levy et al.*, 1996, 1999; *Kasibhatla et al.*, 2000; *Schultz et al.*, 2000]. Thus much effort has been invested in field campaigns to characterize the regional distribution and chemical interactions of tropospheric trace species that are components of the photochemistry involving O_3 and its precursors (see *Emmons et al.* [2000] and references therein for examples). Assessments of these regional chemical environments via techniques such as diel steady state box model analyses give values for regional photochemical tendencies of O_3, which is an important component in the overall O_3 budget.

While human populations in tropical regions do not generate the magnitude of fossil fuel industrial emissions that are prevalent at northern hemispheric (NH) middle latitudes, the tropical troposphere is significantly impacted by large-scale seasonal biomass burning. The local rate of O_3 production near regions of large-scale burning can be comparable to that over industrialized regions at temperate middle latitudes during summertime [*Fishman et al.*, 1985; *Fishman et al.*, 1996; *Jacob et al.*, 1996]. Recognizing the important contribution of tropical regions to global photochemistry, several NASA Global Tropospheric Experiment (GTE) field campaigns have been conducted over tropical and subtropical regions to assess the chemical state of the tropical troposphere, including studies both over areas far from human influence and intensive field campaigns over continental regions directly impacted by human activity [e.g., *Davis*, 1980; *Harriss et al.*, 1988, 1990; *Gregory et al.*, 1986; *Fishman et al.*,1996; *Hoell et al.*, 1997, 1999]. The NASA Transport and Atmospheric Chemistry Near the Equator - Atlantic (TRACE-A) aircraft campaign was conducted over the southern Atlantic basin during the height of the Southern Hemisphere burning season in South America and Africa. Observations from this campaign confirmed that biomass burning emissions create a seasonal doubling of tropospheric O_3 over the tropical South Atlantic [*Olson et al.*, 1996; *Thompson et al.*, 1996]. *Fishman et al.* [1991] suggested that the impact of large-scale biomass burning on O_3 could reach hemispheric scales.

The GTE Pacific Exploratory Mission - Tropics A (PEM-Tropics A) field campaign, conducted in September and October of 1996 [*Hoell et al.*, 1999], provided an opportunity to assess the impact of biomass burning on the remote southern Pacific. Indeed, major findings from PEM-Tropics A included the documentation of the widespread influence of the advection of biomass burning pollution into the South Pacific from fires in Australia, Africa, Indonesia, and possibly even South America [e.g,. *Blake et al.*, 1999; *Dibb et al.*, 1999; *Olson et al.*, 1999]. Additionally, the South Pacific Convergence Zone (SPCZ) was identified as a barrier for atmospheric transport, with the most polluted air masses generally contained to latitudes south of the SPCZ [*Board et al.*, 1999; *Fenn et al.*, 1999; *Fuelberg et al.*, 1999; *Gregory et al.*, 1999]. *Schultz et al.* [1999] examined the O_3 budget for the PEM-Tropics A period, and in contrast to the near chemical balance found over the tropical Atlantic during TRACE-A [*Jacob et al.*, 1996], they calculated a net loss over the tropics and subtropics of -1.5×10^{11} molecules cm^{-2} s^{-1} for the South Pacific. *Schultz et al.* [1999] suggested that the budget of O_3 over the South Pacific could be closed by westerly advection of O_3 into the Pacific from regions of tropical biomass burning.

PEM-Tropics B was conducted during March and April of 1999, again focusing on the remote equatorial and South Pacific [*Raper et al.*, this issue]. One of the primary goals of the dual mission combination PEM-Tropics A and PEM-Tropics B was to enable a seasonal comparison of meteorological and chemical conditions over this previously data-sparse region.

This study uses a time-dependent photochemical box model to examine photochemistry over the South Pacific during the two PEM-Tropics campaigns and, in particular, to identify seasonal characteristics of the O_3 budget based on the in situ information from the wet and dry seasons. A description of the observational database used in this study and a discussion of observed chemical features is presented in section 2. Section 3 describes the time-dependent box model and the modeling approach. The presentation and discussion of results is in section 4, which includes model-to-measurement intercomparisons of HO_x (HO_x = OH +HO_2) and NO_x, and discussions of the photochemistry of HO_x, NO_x, peroxides, and O_3. The major conclusions of this study are summarized in section 5.

2. Observational Database and General Features

During the two PEM-Tropics campaigns, measurements of a suite of chemical species were obtained from the DC-8 aircraft. The DC-8 has a nominal ceiling of 12 km, and flight paths during the two campaigns spanned from 150°E to 90°W in longitude over the equatorial Pacific. DC-8 flight paths over the area of interest for this study during both campaigns are shown in Figure 1.

Measurements from the DC-8 for both missions include NO, NO_2, PAN, HNO_3, CO, O_3, peroxides, hydrocarbons, and several other species as well as measurements of physical parameters such as temperature, humidity, altitude, aerosol number and size distributions, and the spectral actinic flux. During PEM-Tropics B, additional measurements of the critical photochemical species OH and HO_2 are also available [*Tan et al.*, this issue]. Details on the instruments and measurements obtained during PEM-Tropics A are given by *Hoell et al.* [1999] and by *Raper et al.* [this issue] for PEM-Tropics B. In this study, we focus on seasonal differences in the photochemical environment of the tropical and the southern subtropical Pacific from 10°N to 30°S as implied by data from the two campaigns. All data presented here have been merged into 1-min averages for modeling and analysis purposes, as described by *Schultz et al.* [1999]. General regional characteristics over tropical (10°N-10°S) and southern subtropical (10°-30°S) latitudes for each campaign are listed in Table 1.

Figure 2 shows latitude plots for CO and O_3 during PEM-Tropics A and PEM-Tropics B. Constituent distributions obtained during the Southern Hemisphere (SH) dry season PEM-Tropics A campaign displayed a geographic distinction at the approximate location of the SPCZ between the cleaner tropics and the southern subtropical regions where biomass burning pollution plumes were frequently encountered [*Blake et al.*, 1999; *Board et al.*, 1999; *Dibb et al.*, 1999; *Fenn et al.*, 1999; *Fuelberg et al.*, 1999; *Gregory et al.*, 1999]. This is evident in Figures 2a and 2c, with O_3 and CO south of 10°S showing enhanced concentrations relative to data north of that latitude. Alternately,

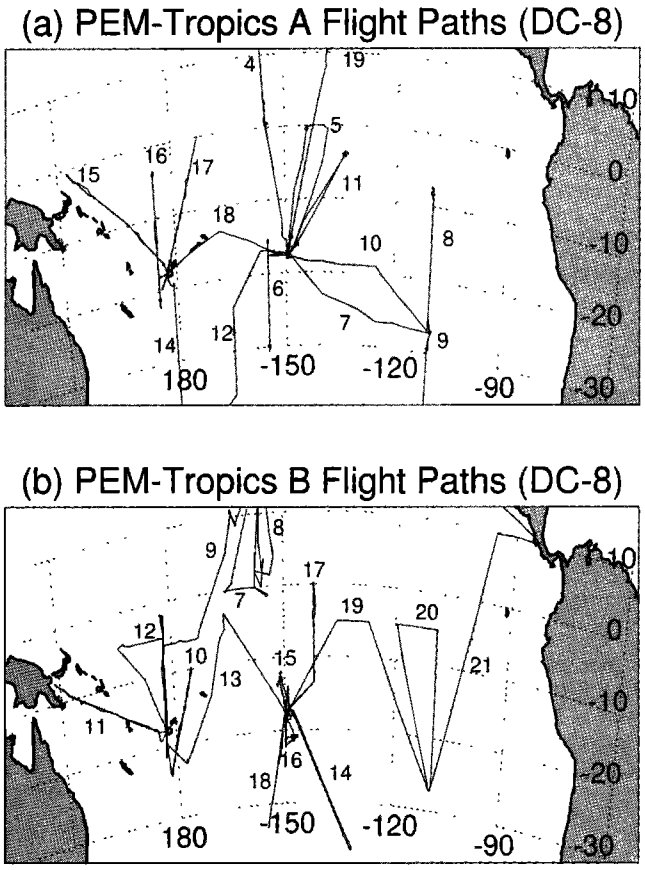

Figure 1. Flight paths for the DC-8 aircraft during the (a) PEM-Tropics A and (b) PEM-Tropics B field campaigns. Numbers indicate the individual flight numbers.

Figures 2b and 2d show the cleaner and more remote conditions encountered during PEM-Tropics B (March 1999).

Baseline tropospheric CO for the southern subtropics (10°-30°S) decreases from 50 ppbv during September (PEM-Tropics A) to 38 ppbv during March (PEM-Tropics B), shown by the dashed lines in Figures 2a and 2b. Here the baseline is defined as that concentration representing the fifth percentile of the data. Similar seasonality is also seen for species such as C_2H_6 and C_3H_8 (not shown). The baseline CO values are in close agreement with time series data from several far remote SH sites over Antarctica and from Cape Grim, Tasmania [*Novelli et al.*, 1998]. Data from PEM-Tropics B were obtained during March, at the end of the photochemically active SH summer season when CO loss to OH is maximized in the SH middle latitudes, so the lower baseline value during March reflects, in part, the general hemispheric photochemical cycle for the CO loss rate. Additionally, *Novelli et al.* [1998] argue that the hemispheric seasonal cycle of background CO is also greatly influenced by the seasonality of biomass burning emissions, which maximize during the Southern Hemisphere austral spring (roughly August through October).

Latitudinal distributions of O_3 in Figure 2 also show clear evidence of the influence of biomass burning pollution in the southern subtropical latitudes, with much higher variability of concentrations evident during the PEM-Tropics A burning season (Figure 2c) compared to the PEM-Tropics B wet season (Figure 2d). For the subtropical latitudes 10°-30°S, the inner quartile for O_3 data was between 31 and 63 ppbv during PEM-Tropics A, while the equivalent range is roughly half during PEM-Tropics B at 17 and 27 ppbv. Additionally, very low O_3 values within the tropical boundary layer were encountered more often during PEM-Tropics B than during PEM-Tropics A. Over the tropical latitudes (10°N-10°S), median boundary layer O_3 below 1 km equals 14 ppbv during September and is nearly half that at 7.5 ppbv during March (PEM-Tropics B).

2.1. Tropics (10°N-10°S)

Median profiles for various constituents within the tropics are shown in Figure 3 for each campaign. The bars show the inner quartile of the data and the lines indicate the inner 90% of the data at each altitude level. The tropical troposphere contains higher concentrations of O_3 during September (PEM-Tropics A) at all altitudes (Figure 3b). Integrated from 0 to 12 km, the median tropospheric O_3 column amount is nearly 15 DU during September and is 11.3 DU during March (PEM-Tropics B; See Table 1). Median concentrations of tropical NO_x are also larger during September (PEM-Tropics A) above 4 km, with similar concentrations during the two seasons below that altitude where NO_x lifetimes are less than a day (Figure 3d). The high scatter of lower altitude NO_x during PEM-Tropics B is influenced by sampling of northern hemispheric air masses during flights right at the 10°N boundary; median values are not significantly altered by these data points. Upper tropospheric CO shows a similar seasonality to that for O_3 and NO_x; median values during September (PEM-Tropics A) are 5-10 ppbv higher than those during March (PEM-Tropics B; Figure 3c). In contrast, however, the seasonality of CO reverses below 4 km; at these altitudes, median concentrations are largest during PEM-Tropics B, although a much broader range of values are encountered. These lower tropospheric concentrations reflect the influence of low altitude transport of NH middle latitude air into the tropics during PEM-Tropics B [*Avery et al.*, this issue; *Fuelberg et al.*, this issue]. Median water vapor mixing ratios for the two seasons are quite similar below 8 km (within 10%), with the exception of the very low concentration at 4-6 km for the PEM-Tropics A data.

In constructing median observations from a data set such as

Table 1. Characteristics of Selected Regions During the PEM-Tropics A and B Campaigns

	PEM-Tropics A Tropics (West of 180°, East of 180°)		PEM-Tropics B Tropics	PEM-Tropics A Subtropics	PEM-Tropics B Subtropics
Number of data points	896	(344, 552)	1496	1581	1552
Median latitude	4.2°S	(5.6°S, 3°S)	1.9°S	17.6°S	15.5°S
Median column H_2O (10^{22} molec cm^{-2}), 0-2 km	9.4	(10.7, 8.8)	9.8	6.6	8 3
Median column H_2O (10^{22} molec cm^{-2}), 2-8 km	3.8	(5.8, 2.6)	4.4	0.78	2 8
Median tropospheric O_3 column (DU), 0-12 km	14.8	(12.3, 18.2)	11.3	28.3	12.7
Median TOMS O_3 (DU)	258	(255, 259)	264	280	259

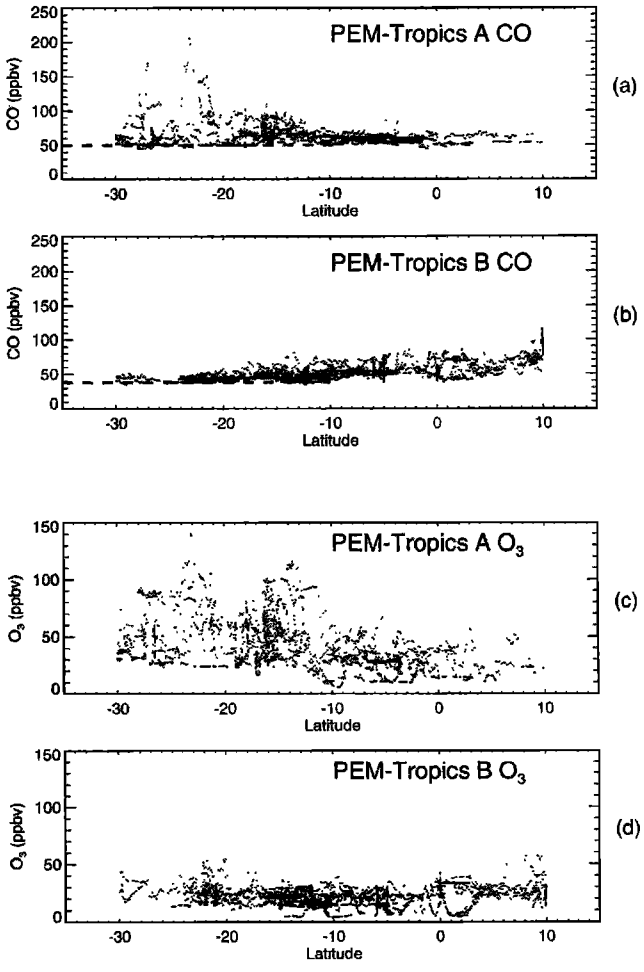

Figure 2. Latitudinal distribution of CO and O_3 during the PEM-Tropics A and PEM-Tropics B field campaigns. The data shown are the subset of the 1-min merged data set used for modeling (see discussion in text). Baseline values (5th data percentile) for CO over the subtropical latitudes 10°-30°S are indicated by dashed lines in Figures 2a and 2b.

from these aircraft campaigns, it is important to ensure that sampling biases do not influence the statistics of the data. To test for sampling biases during the PEM-Tropics campaigns, measurements were weighted equally by event, where an event is defined as a flight leg or a single ascent or descent within an altitude regime. For the species profiles shown in Figure 3, sampling biases had a negligible impact on the median values with the exception of water vapor during PEM-Tropics A. Asterisks in Figure 3a indicate H_2O event medians during PEM-Tropics A. Note that the 4-6 km event median H_2O during PEM-Tropics A is 2200 ppmv, compared to the 750 ppmv full median value. More than a third of the data obtained at this altitude was from a single flight leg on Flight 11 (see Figure 1a), which encountered a very dry air mass. Median concentrations for species such as O_3, CO, and NO_x were not similarly impacted by this flight leg, however. Thus, while we retain the full medians for the analysis presented in this study, we acknowledge that the very low median water vapor at 4-6 km (and to a lesser extent at 8-10 km) is likely to be somewhat skewed by sampling biases.

Climatological streamline analysis for the PEM-Tropics A period of September 1996 shows a center of anticyclonic circulation present at the lower altitudes over the eastern Pacific around 20°S [*Fuelberg et al.*, 1999] which facilitates flow of polluted subtropical air into the eastern equatorial region at lower and middle tropospheric altitudes around the anticyclone, followed by easterly flow across the tropics. At upper altitudes, this type of transport regime breaks down. In fact, the PEM-Tropics A data do suggest a longitudinal gradient below 8 km over the tropics which is consistent with this scenario, with higher O_3, CO, and NMHC and lower water vapor in the eastern tropics compared to data in the cleaner far western reaches of the campaign region (Table 1). For example, median integrated 0-12 km column O_3 is 50% larger in the eastern PEM-Tropics A tropics than for longitudes west of 180°. Water vapor shows the opposite gradient: below 2 km, median water vapor is 20% larger in the west compared to that in the east and remains significantly larger over the west throughout the middle troposphere.

2.2. Subtropics (10°-30°S)

Figure 4 shows constituent profiles over the subtropical regions. Median water vapor during the dry season (PEM-Tropics A) is persistently lower at all altitudes than during PEM-Tropics B (Figure 4a), with frequent sampling of dry air relative to the March data (PEM-Tropics B), particularly in the middle troposphere. H_2O concentrations during PEM-Tropics A are 20% lower in the lowest 2 km and are 75% lower at middle and upper altitudes.

For this latitude regime, a more distinct seasonal difference is observed in chemical constituents, with highest median concentrations of O_3, CO, and NO_x during September (PEM-Tropics A) (Figures 4b-4d). Integrated O_3 is more than twice as abundant during PEM-Tropics A relative to PEM-Tropics B (Table 1), and CO is consistently 15-20 ppbv larger throughout the troposphere (Figure 4c). Above the boundary layer, median NO_x is enhanced by factors of between 2 and 5 relative to PEM-Tropics B (Figure 4d). Additionally, these species all uniformly show an increased range of scatter during the September burning season (PEM-Tropics A). The differences between the subtropical constituent profiles between March (PEM-Tropics B) and September (PEM-Tropics A) are consistent with the influence of biomass burning emissions transported into the southern Pacific during the Southern Hemisphere burning season.

Event median values showed little to no discernible differences from full medians for the PEM-Tropics B data set. During PEM-Tropics A at altitudes above 6 km, differences between event and full medians were somewhat more variable, although in most cases, differences were less than 20%. The use of event medians had no significant impact on the integrated regional photochemical results, however.

3. Model Description

The analyses presented here are based on calculations from a time-dependent photochemical box model. This model has been described in detail in several previous studies, the most recent of which is *Crawford et al.* [1999]. Basic HO_x-NO_x-CH_4 gas phase chemistry is included with reactions and rates based on the recommendations of *DeMore et al.* [1997] and *Atkinson et al.* [1992]. Nonmethane hydrocarbon (NMHC) chemistry is based on the condensed mechanism of *Lurmann et al.* [1986] with modifications included to address remote low-NO_x conditions (e.g., formation of organic peroxides) and to represent explicit chemistry for acetone, propane, and benzene. Heterogeneous loss

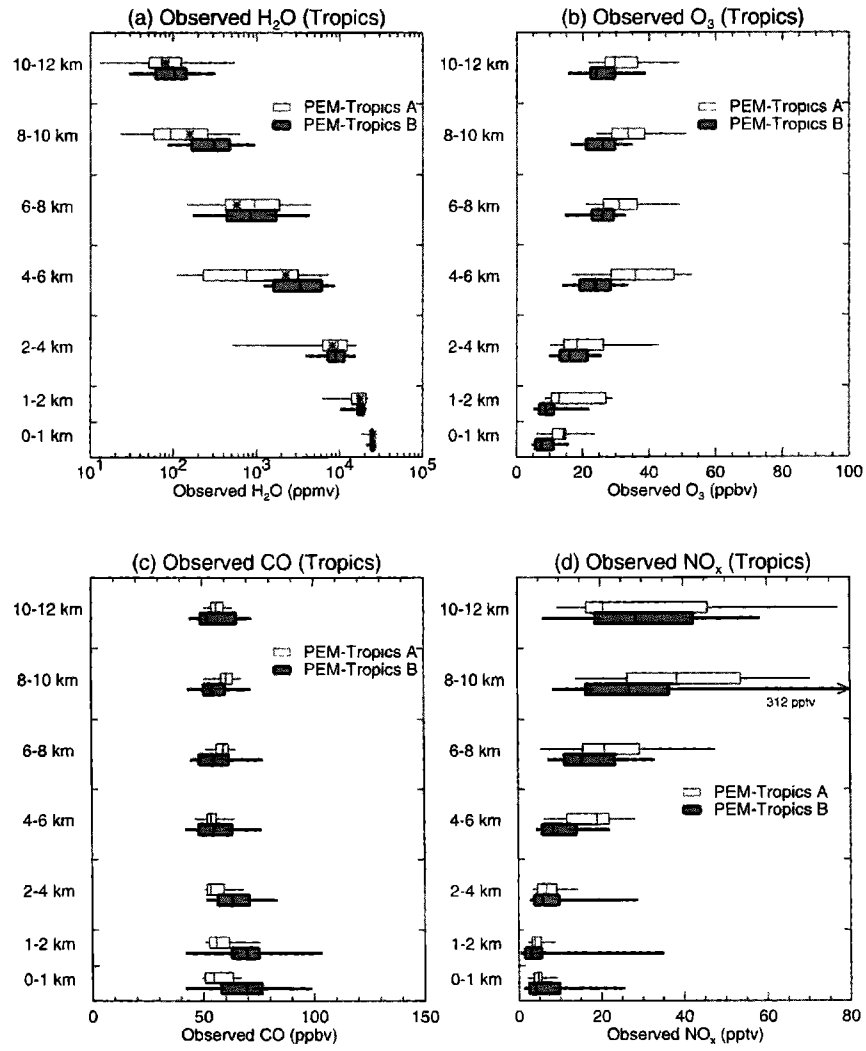

Figure 3. Box-line plots of key constituent observations over tropical latitudes (10°N-10°S) during PEM-Tropics A (open) and PEM-Tropics B (shaded). The data shown are the subset of the 1-min merged data set used for modeling (see discussion in text). Data are segregated by altitude (vertical axis), where boxes denote the inner quartile of the data for each altitude level, and lines denote the inner 90th percentile . Medians are indicated by the center lines within the boxes. Asterisks in Figure 3a represent the event medians for H_2O during PEM-Tropics A (see discussion in text).

for soluble species is from *Logan et al.* [1981]. A detailed listing of reactions and rate coefficients is included in the appendix given by *Crawford et al.* [1999].

Model calculations are based on the 1-min merged data set described previously and are constrained by observations of O_3, CO, NO, NMHCs, acetone, temperature, dew/frost point, and pressure. Because the model analyses are critically dependent on the availability of these constraining species, only a subset of the full data merge can be used. Thus gaps of missing NMHC and acetone data are interpolated across data gaps of less than 5 min. Otherwise, NMHC gaps are filled with altitude-dependent median values. In addition, these analyses were limited to conditions with solar zenith angles less than 75°, and data that were clearly stratospheric were eliminated. For PEM-Tropics B, 3048 points, or 45%, of the 1-min merged points within the 10°N to 30°S latitude range are analyzed. For PEM-Tropics A, 2477 points, or 43%, of the merged points within the latitude range are used. Table 1 includes the number of the merged data points utilized within the tropics (10°N-10°S) and southern subtropics (10°-30°S) for each campaign.

In addition to the critical constraining species described above, model calculations are also constrained by H_2O_2, CH_3OOH, HNO_3, PAN, CH_3OH, and C_2H_5OH when measurements are available; otherwise, these species are calculated by the model. With the exception of NO, constraining parameters are assumed to remain constant over the diurnal cycle. NO is allowed to vary diurnally; however, total short-lived nitrogen ($NO+NO_2+NO_3+2N_2O_5+HONO+HNO_4$) is held constant. The amount of short-lived nitrogen is determined such that the NO concentration matches the measurement at the appropriate time of day. Photochemistry dictates the partitioning of short-lived nitrogen among the constituent species. While observed NO_2 was not used as a constraining species in the model runs, a comparison of measured and model-predicted values was used to assess the adequacy of the simulated NO_x photochemistry.

Model-calculated species are assumed to be at steady state,

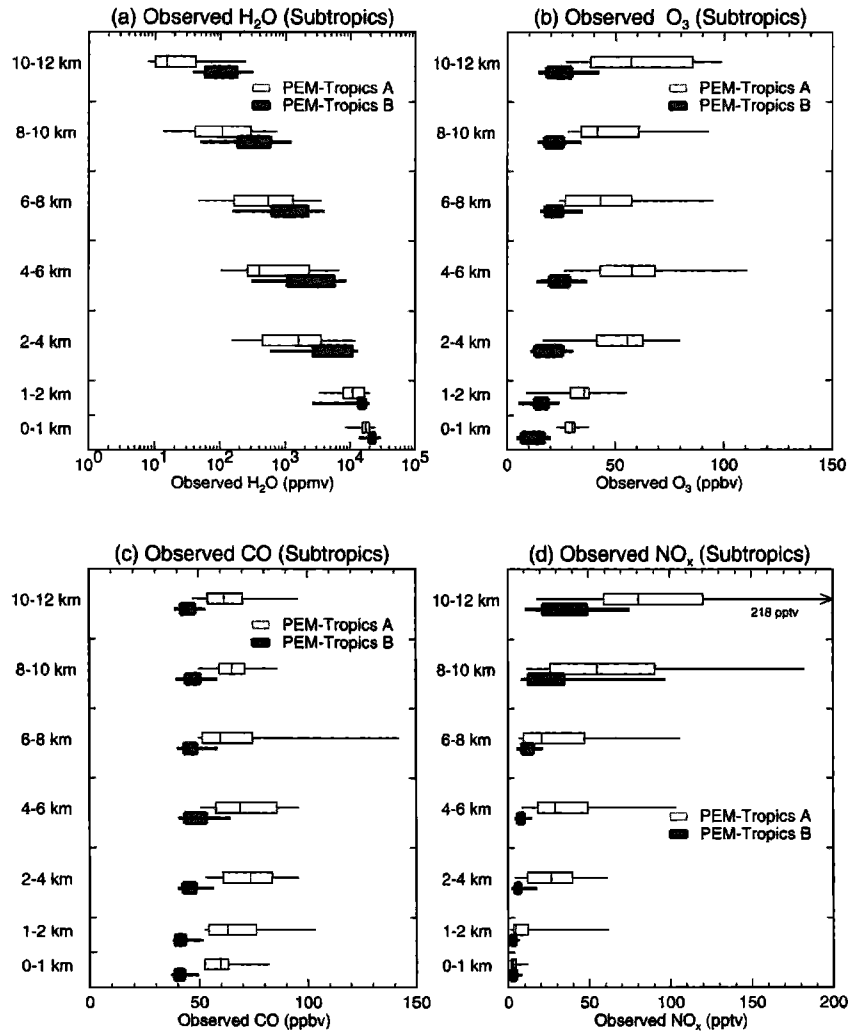

Figure 4. Box-line plots of key constituent observations over subtropical latitudes (10°-30°S) during PEM-Tropics A (open) and PEM-Tropics B (shaded). See Figure 3 for data and box-line definitions.

meaning that concentrations are integrated in time until their diurnal cycles no longer vary from day to day. Photolysis rate coefficients are computed using a DISORT four-stream implementation of the NCAR Tropospheric Ultraviolet Visible (TUV) radiative transfer code. Rate coefficients are initially based on a clear-sky assumption and are then adjusted to account for cloudiness conditions, depending on the type of model simulation. For purposes of direct model to measurement intercomparisons, the model is run in an instantaneous mode, whereby the model clear-sky photolysis rates are normalized throughout the day such that in situ spectroradiometer photolysis measurements are exactly matched at the time of the measurement [*Shetter and Müller*, 1999; *R.S. Shetter et al.*, manuscript in preparation, 2001]. Diurnally averaged output are presented for issues involving photochemical tendency terms (e.g., O_3 budget analysis). Recognizing that instantaneous cloud conditions that impact in situ measurements do not accurately represent diurnally averaged conditions, the model clear-sky photolysis coefficients for these cases are adjusted at each time step with a climatological cloud correction factor (CCF). As for past PEM studies, the CCF is determined by taking the mission median of the ratio of the observed photolysis rates to modeled instantaneous clear-sky calculations as a function of altitude. For both PEM-Tropics campaigns, the boundary layer CCF was significantly different from 1 (0.93 for PEM-Tropics A and 0.9 for PEM-Tropics B). Above the boundary layer, the CCF varied around 1 by less than +/- 4%, depending on the altitude.

4. Model Results

4.1. HO_x

4.1.1. Model and measurement comparisons. The availability of in situ HO_2 and OH measurements on board the DC-8 during PEM-Tropics B provides a direct measure of a model's ability to assess the photochemical environment for a given set of input conditions. Recent studies which have similarly used a combination of measurements and models have indicated that models tend to underpredict HO_2 in the upper troposphere and have suggested that species such as acetone and peroxides may be a potentially important source of upper tropospheric HO_x [*Wennberg et al.*, 1998; *Jaeglé et al.*, 1997, 1998; *McKeen et al.*, 1997; *Brune et al.*, 1998]. *Tan et al.* [this issue] describes the HO_x measurements that were obtained during this mission, and detailed analyses on aspects of the HO_x budget and model-to-measurements comparisons can also be found in J.M. Rodriguez et al. (manuscript in preparation, 2001).

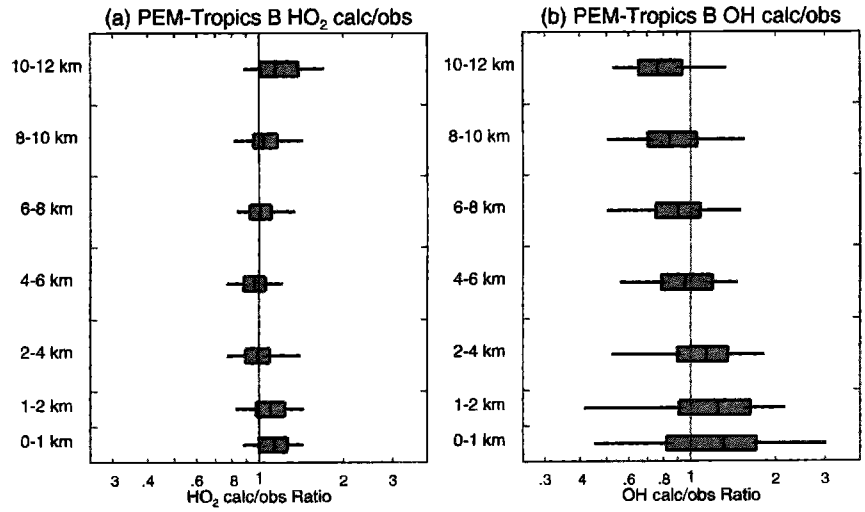

Figure 5. Box-line plots of the model-calculated to observed ratios for (a) HO_2 and (b) OH for all latitudes considered here (10°N-30°S) during PEM-Tropics B. The data shown are the subset of the 1-min merged data set used for modeling (see discussion in text) which contains valid HO_x measurements. See Figure 3 for box-line definition.

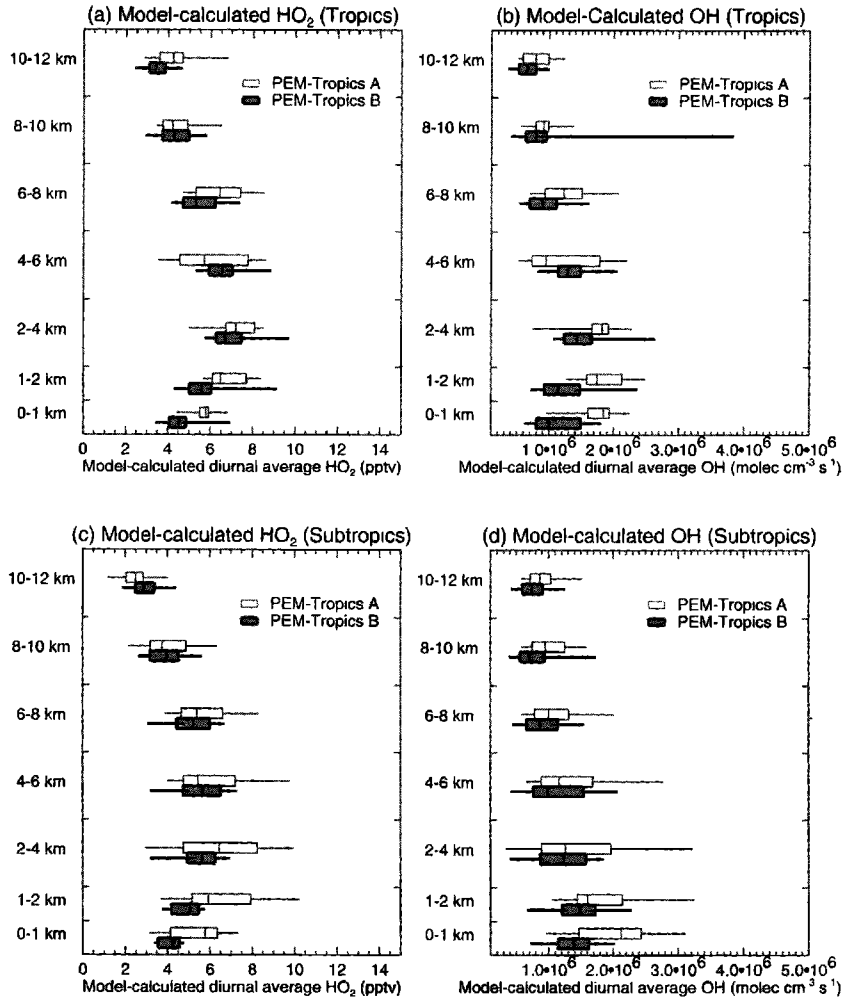

Figure 6. Box-line plots of model-predicted diurnal averages for tropical (a) HO_2 and (b) OH and for subtropical (c) HO_2 and (d) OH during PEM-Tropics A (open) and PEM-Tropics B (shaded). See Figure 3 for data and box-line definitions.

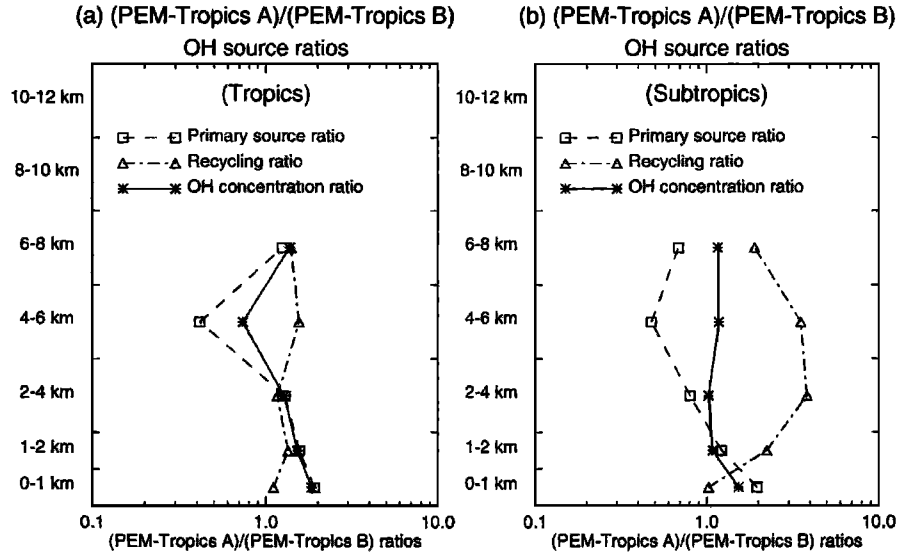

Figure 7. PEM-Tropics A to PEM-Tropics B ratios for median model-predicated diurnal average OH sources for (a) tropical latitudes (10°N-10°S) and (b) subtropical latitudes (10°-30°S). Squares and dashed lines show the PEM-Tropics A/PEM-Tropics B ratio for the median primary OH source (H_2O+O^1D). Triangles and dash-dotted lines show the PEM-Tropics A/PEM-Tropics B ratio for the HO_x recycling source of OH (HO_2+NO). Also shown are the PEM-Tropics A/PEM-Tropics B ratios of the median model-predicted OH concentrations (asterisks and solid line).

In contrast to the previous mentioned studies, this box model analysis indicates that calculated HO_2 is larger than observed in the upper troposphere during PEM-Tropics B. Figure 5 shows the median calculated-to-observed ratios (calc/obs) for HO_2 and OH as a function of altitude for the entirety of the tropical and subtropical data set used here. The overall agreement is good, with a median value of 1.03 for HO_2 and 0.91 for OH. However, there is a tendency toward overprediction of HO_2 in the upper troposphere with a coincident underprediction of OH. At altitudes above 8 km, the median HO_2 calc/obs ratio is 1.08, while the median OH calc/obs ratio is 0.80. As a result, the OH/HO_2 ratio is underpredicted by ~30%. Alternately, HO_x is overpredicted in general below 2 km, by 12% for HO_2 and 30% for OH. The OH/HO_2 ratio is overpredicted at these low altitudes by ~10%. While both OH and HO_2 have a reported accuracy of +/- 40%, the broader range of ratios for OH reflects the lower precision for this species which is derived from a much smaller signal than for HO_2 [*Faloona et al.*, 2000].

4.1.2. Predicted HO_x seasonality. Figure 6 shows model-predicted, diurnally averaged HO_2 and OH concentrations. Lower tropospheric (< 4 km) concentrations of HO_2 and OH are uniformly larger during PEM-Tropics A relative to PEM-Tropics B. Additionally, upper tropospheric OH is 15-30% larger during PEM-Tropics A at both latitudinal expanses. While upper tropospheric HO_2 is generally larger during September (PEM-Tropics A) relative to March (PEM-Tropics B) over the tropics, little seasonality is evident over the subtropics (Figures 6a and 6c).

To a first order, formation of OH results from the primary HO_x source ($O^1D+H_2O\rightarrow 2OH$) and also from the recycling of HO_2 to OH, largely via NO_x ($HO_2+NO\rightarrow OH+NO_2$). Examination of the relative strengths and seasonality of these terms can shed some insight on the seasonality of the HO_x profiles shown in Figure 6 and ultimately can assist interpretation of the performance of models in accurately predicting HO_x under various controlling conditions.

Figure 7 shows seasonal changes in the form of a ratio (PEM-Tropics A/PEM-Tropics B) for the model-predicted median primary OH source ($O^1D+H_2O\rightarrow 2OH$; squares and dashed lines) and for the median recycling OH source ($HO_2+NO\rightarrow OH+NO_2$; triangles and dash-dotted lines). The profiles in Figure 7 are limited to altitudes below 8 km because primary HO_x sources from species other than water vapor become significant in the dry upper troposphere [*Wennberg et al.*, 1998; *Jaeglé et al.*, 1997, 1998; *McKeen et al.*, 1997; *Brune et al.*, 1998; *Crawford et al.*, 1999]. Figure 7 also shows the seasonal changes in median OH concentrations predicted by the model ($OH_{PEM\text{-}Tropics\ A}/OH_{PEM\text{-}Tropics\ B}$) (asterisks and solid lines). In the lowest 2 km, where the primary source dominates recycling by more than an order of magnitude, seasonal changes in OH at both latitude regimes are closely correlated to seasonal changes in the primary source, while seasonality in the strength of the recycling term has a negligible impact. Above 2 km in the subtropics, where the relative importance of the recycling reaction is increased in the higher NO_x environment during PEM-Tropics A, the seasonal change in OH loses its correlation with the primary source and instead reflects a combination of the seasonality for both the primary source and the recycling terms. Thus while the primary source term for HO_x is 30-50% lower during the subtropical dry season (PEM-Tropics A) in the middle troposphere (evidenced by PEM-Tropics A/PEM-Tropics B ratio values < 0.7 in Figure 7b), OH concentrations do not correspondingly decrease and in fact slightly increase as a result of the up to four-fold increase in the recycling source term (also shown in Figure 7b). Alternately, over the lower NO_x environment of the tropics, the seasonal change in OH retains a fairly close correlation to seasonality in the primary source through the lower and middle troposphere (Figure 7a).

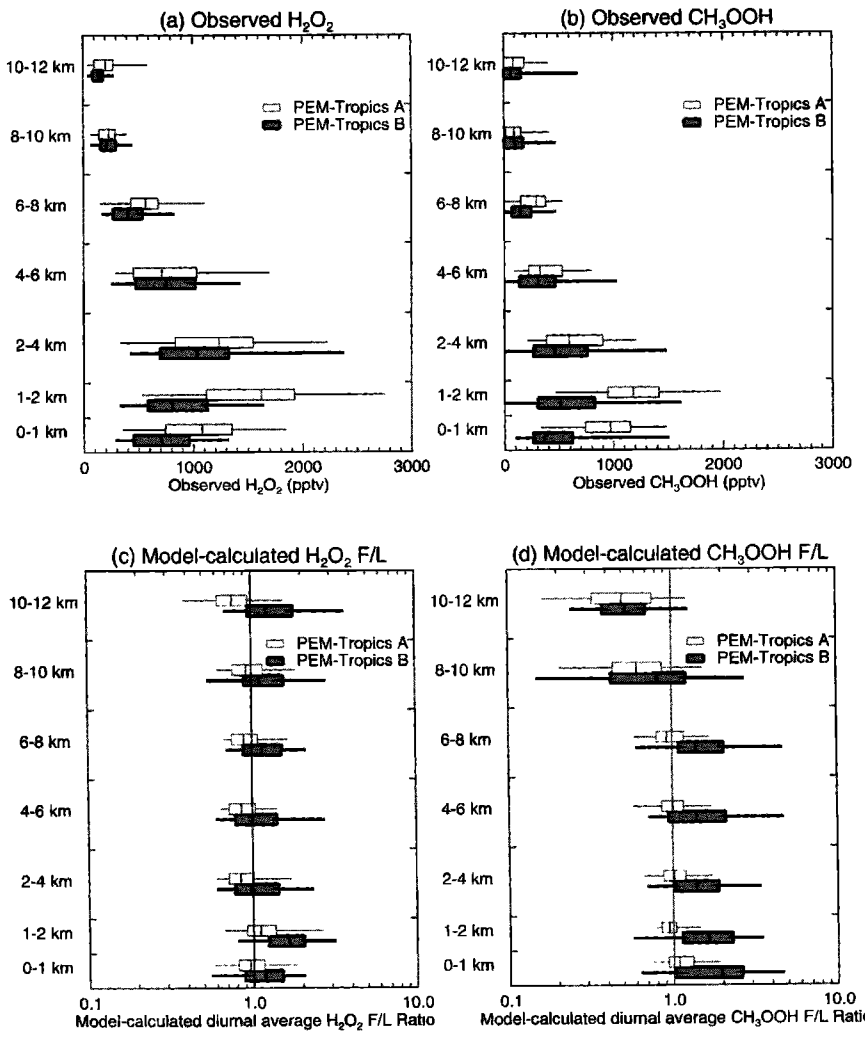

Figure 8. Box-line plots of observations of (a) H_2O_2 and (b) CH_3OOH for all latitudes considered here (10°N-30°S) during PEM-Tropics A (open) and PEM-Tropics B (shaded). The data shown are the subset of the 1-min merged data set used for modeling (see discussion in text) which contains valid peroxide measurements. See Figure 3 for box-line definition. Also shown are the model-calculated diurnal average formation to loss ratios (F/L) for (c) H_2O_2 and (d) CH_3OOH. For these calculations, data are further limited to those points where peroxide observations are above the limit of detection.

4.2. Peroxides

The peroxides H_2O_2 and CH_3OOH result from the reaction of photochemically produced radicals HO_2 and CH_3O_2. They also have fairly short lifetimes ranging from less than a day to a few days. Thus the abundance of these photochemically derived species represents another useful diagnostic for the model's representation of local photochemical activity. The altitude distributions for H_2O_2 and CH_3OOH during PEM-Tropics A and PEM-Tropics B are shown in Figures 8a and 8b. H_2O_2 distributions show the greatest difference below 2 km, with PEM-Tropics A showing significantly larger median values. Differences above 2 km are much smaller, although median values for PEM-Tropics A still tend to be greater. A similar situation exists for CH_3OOH which shows median values for PEM-Tropics A to be roughly double those for PEM-Tropics B below 2 km. Again, differences above 2 km are rather small. These differences are qualitatively consistent with the calculated seasonal HO_2 distributions showing greater abundances in the lower troposphere during PEM-Tropics A (see Figure 6). A more rigorous assessment, however, shows that the model calculations are unable to account for the seasonal differences observed in the peroxide distributions.

Figures 8c and 8d examine the balance between peroxide formation and loss. Given their short lifetime, the assumption of steady state for peroxides (i.e., formation equals loss) should be valid in general. However, it is recognized that for individual observations, recent wet removal in precipitation or changes in photochemical environment can lead to significant deviations from steady state. Overall, formation and loss of H_2O_2 is fairly well represented by the model with most median formation to loss ratios (F/L) falling within 20% of unity. Below 2 km, F/L ratios for H_2O_2 are more consistent with the observations for PEM-Tropics A, while F/L ratios for PEM-Tropics B indicate that the model is predicting more H_2O_2 than is being observed. From 2 to 6 km, the model is more consistent with PEM-Tropics B data, and above 6 km, the model underpredicts PEM-Tropics

A observations and overpredicts PEM-Tropics B observations. Despite these trends, the consistency between observations and model calculations must be considered equally good during both seasons.

Unlike H_2O_2, calculations of formation and loss show a distinct trend in agreement with observations of CH_3OOH (Figure 8d). Below 8 km, median F/L ratios for PEM-Tropics A fall within 10% of unity, while median ratios for PEM-Tropics B tend to be 1.5 or greater. Even the lower quartile ratio is typically 1 or greater, indicating that model calculations of CH_3OOH for PEM-Tropics B consistently exceed observed values. The range of F/L values for PEM-Tropics B is also much broader than for PEM-Tropics A at these altitudes. Above 8 km, median ratios for both PEM-Tropics A and PEM-Tropics B are less than 1. As noted in previous studies, this is consistent with the convective transport of CH_3OOH from the marine boundary layer enhancing CH_3OOH above expected steady state values [*Jaeglé et al.*, 1997; *Prather and Jacob*, 1997; *Cohan et al.*, 1999; *Schultz et al.*, 1999]. Further evidence for convective perturbation of CH_3OOH and other marine boundary layer tracers are presented by J. Snow et al. (manuscript in preparation, 2001). In addition to convective transport, uncertainties in the CH_3O_2+HO_2 rate constant for the cold temperatures of the upper troposphere have also been cited as a possible contributor to this disagreement [*Jacob et al.*, 1996; *Schultz et al.*, 1999]. It should also be noted that the F/L ratios shown in Figure 8 are calculated from the subset of data including CH_3OOH observations that were greater than the reported limit-of-detection (LOD) value of 25 pptv (J. Snow et al., manuscript in preparation, 2001). A significant fraction of CH_3OOH observations fall below the LOD value above 8 km; at these altitudes, 30% of CH_3OOH data were below LOD during PEM-Tropics A versus 37% for PEM-Tropics B. Therefore F/L distributions do not represent the overall conditions for the upper troposphere.

4.3. NO_x

4.3.1. NO_2. NO_x measurements from early GTE missions indicated a systematic offset between model-calculated and observed NO_2 of the order of between 50% to more than a factor of 3, which suggested uncertainties either in the measurement or in the state of understanding of NO_x photochemistry simulated in models [*Chameides et al.*, 1990; *Davis et al.*, 1993; *Crawford et al.*, 1996]. The two photon laser induced fluorescence (TP-LIF) NO_2 measurement technique was modified during PEM-Tropics A to reduce potential interference effects on the measurement [*Bradshaw et al.*, 1999]. These instrument modifications substantially reduced the systematic offset to within 10% during PEM-Tropics A [*Bradshaw et al.*, 1999; *Schultz et al.*, 1999].

The overall NO_2 calculated-to-observed ratios (calc/obs) for the tropical and subtropical data in this study were 1.07 for PEM-Tropics A and 1.03 for PEM-Tropics B, and the altitude dependence of the ratios is shown in Figure 9. Ratios for PEM-Tropics A data are low from the surface to 2 km, with median values as low as 0.6. *Schultz et al.* [1999] suggested that this underprediction could be corrected by the addition of chlorine-catalyzed recycling of NO to NO_2. An alternate, and more likely, explanation is a small offset in the NO measurement [*Bradshaw et al.*, 1999]. The data used to generate the ratios in Figure 9 were limited by the availability of NO_2 measurements. For this subset of data, median NO during PEM-Tropics A was 1.6 pptv. Thus a NO measurement bias of only 0.5 pptv would be enough to explain the discrepancy in the NO_2 calc/obs ratio shown in Figure 9. During PEM-Tropics B, for the subset of data

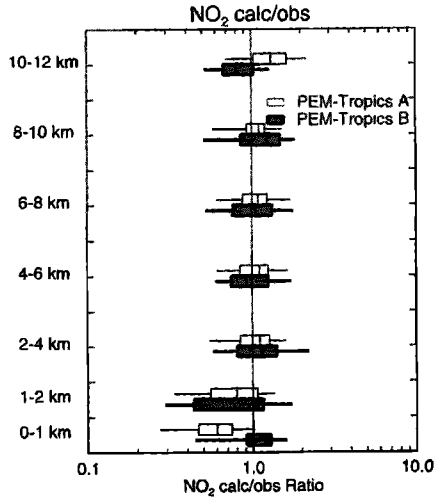

Figure 9. Box-line plots of the model-calculated to observed ratios for NO_2 for all latitudes considered here (10°N-30°S) during PEM-Tropics A (open) and PEM-Tropics B (shaded). The data shown are the subset of the 1-min merged data set used for modeling (see discussion in text) which contains valid NO_2 measurements. See Figure 3 for box-line definition.

including NO_2 measurements, median NO was 5.8 pptv, substantially larger than that during PEM-Tropics A. A small offset in the NO measurement in this case would have a much lower impact on NO_2. This is supported by the PEM-Tropics B NO_2 calc/obs ratios in Figure 9 which show values near unity in the lower troposphere. At middle and upper altitudes, ratios during both campaigns lie well within the range of the stated uncertainties in the measurements [*Bradshaw et al.*, 1999].

4.3.2. NO_x budget. To assess the assumption of a NO_x chemical steady state (i.e., formation equals loss), Figures 10a and 10c show the diurnally averaged NO_x formation to loss ratio (F/L) for altitudes greater than 4 km and for data points which include constraining observations of HNO_3 and PAN. The low median values (0.3-0.5) above 8 km indicate an upper tropospheric source deficit, consistent with previous studies. These low values suggest that models may underpredict the formation of NO_x from recycled species such as HNO_3 and/or that the model inherent assumption of NO_x steady state (i.e., no primary NO_x sources such as from lightning) is invalid [*Jacob et al.*, 1996; *Schultz et al.*, 1999]. It is noteworthy that the underestimates at the upper altitudes are similar for the two seasons at both latitude spans.

Previous studies have reported assessments of NO_x budgets within the lower troposphere and boundary layer and have found that the downward transport of PAN into the lower troposphere and subsequent decomposition is a significant source of NO_x at these low altitudes [e.g, *Jacob et al.*, 1996; *Crawford et al.*, 1997b]. For these studies, NO_x and PAN concentrations in the boundary layer were substantially elevated relative to those found during the PEM-Tropics campaigns. *Schultz et al.* [1999] similarly reported that PAN decomposition was a significant source of NO_x in the lower troposphere during PEM-Tropics A. However, we find that during PEM-Tropics A and PEM-Tropics B, measured values of PAN were so often at or below the instrument LOD that these conditions preclude a lower tropospheric NO_x budget analysis.

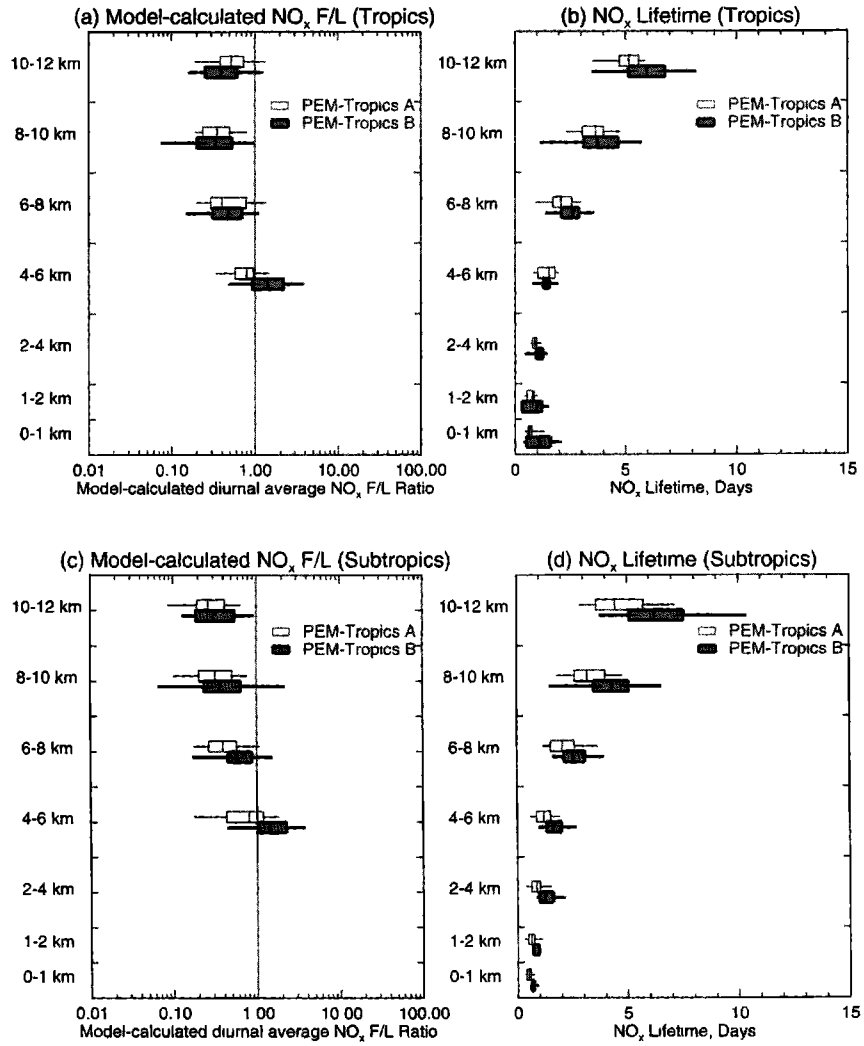

Figure 10. Box-line plots of model-calculated (a) diurnal average formation to loss ratios (F/L) for NO_x at tropical latitudes and (b) NO_x lifetimes at tropical latitudes during PEM-Tropics A (open) and PEM-Tropics B (shaded). Model-calculated diurnal averaged F/L and lifetimes for NO_x at the subtropical latitudes are shown in (c) and (d) respectively. The data shown are the subset of the 1-min merged data set used for modeling (see discussion in text) which contains valid NO_2 measurements. See Figure 3 for box-line definition. F/L ratios are only shown for altitudes greater than 4 km.

NO_x budget calculations are necessarily limited to a subset of the data which includes valid measurements of the NO_x reservoir species HNO_3 and PAN. Under the remote marine conditions encountered during PEM-Tropics A and PEM-Tropics B, this limitation results in a skewed subset of boundary layer data. For example, PAN is reported as LOD more than 80% of the time during PEM-Tropics B (and more than 70% of the time during PEM-Tropics A) in the lowest kilometer at the latitudes considered here. For these instances during PEM-Tropics B, the median model-predicted value for PAN is 0.1 pptv, an order of magnitude lower than the reported LOD value (1 pptv, H. B. Singh, personal communication, 2001). Thus the subset of lower tropospheric data where PAN values were measured above LOD is likely to represent a highly skewed sample of conditions when PAN has been transported into the boundary layer at enhanced concentrations. On the basis of the prevalence of boundary layer LOD measurements of PAN, we suggest that these conditions are unlikely to be typical of the remote marine environment. Subsequent analysis of this subset of data could result in a significant overestimate for the rate of boundary layer NO_x formation via PAN thermal decomposition relative to more typical conditions.

To illustrate, for the PEM-Tropics B data considered in this study, only 27 points contain PAN data greater than LOD in the boundary layer, with a median concentration equal to 2 pptv. The median calculated F/L ratio for these points is 7.3. When we expand the data set to also include points where PAN was measured at LOD (115 additional points), the median F/L ratio drops to 1.2. Note that for these additional points, PAN concentrations are predicted by the model. We acknowledge that the use of F/L as an assessment of steady state conditions without constraining a primary source species such as PAN to observations is not meaningful, but the difference in the predicted median F/L highlights the extent of the impact of limiting the subset of data to points where PAN was measured larger than LOD. We submit that a complete assessment of the NO_x budget

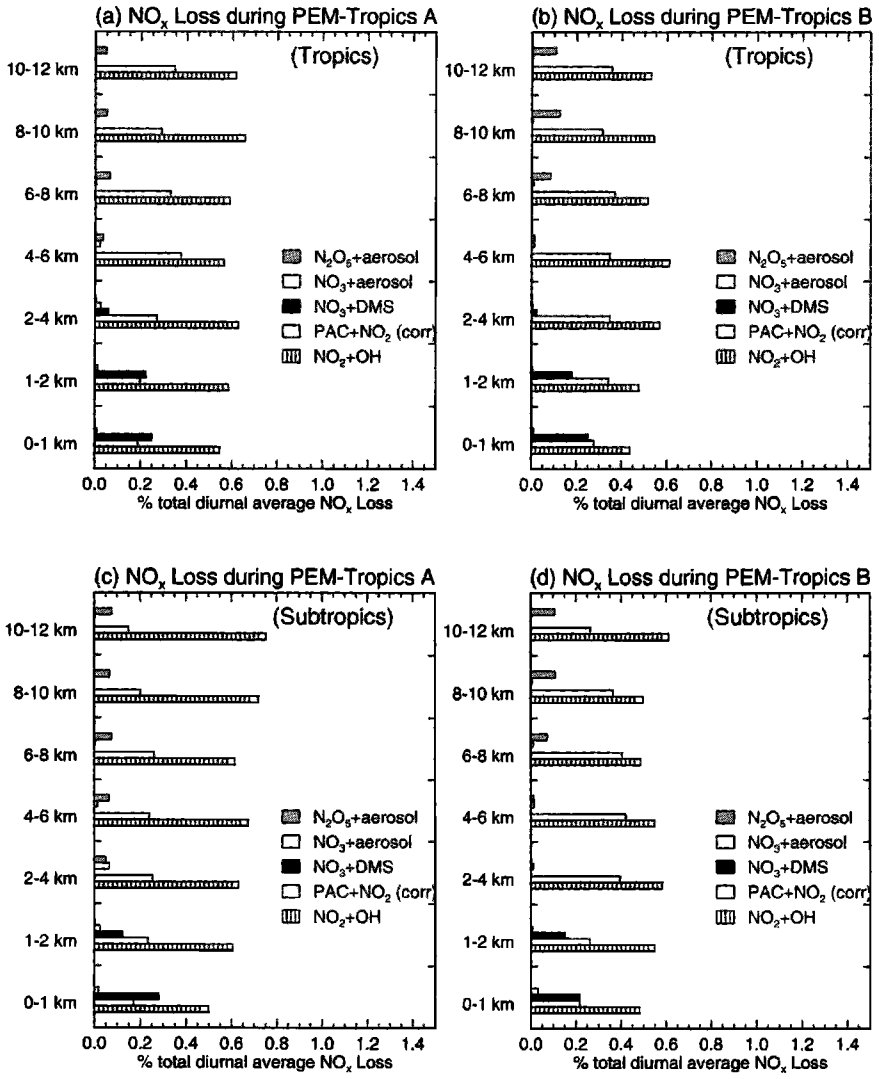

Figure 11. Percentage of the model-calculated, diurnal-average NO_x loss attributable to the individual loss pathways for (a) PEM-Tropics A tropics (10°N-10°S), (b) PEM-Tropics B tropics, (c) PEM-Tropics A subtropics (10°-30°S), and (d) PEM-Tropics B subtropics.

for remote marine boundary layer conditions such as those encountered during PEM-Tropics A and PEM-Tropics B will not be resolvable until we gain the ability to quantify concentrations of PAN at the extremely low values predicted as typical for this environment (< 0.1 pptv).

While the use of the F/L ratio is not meaningful for a boundary layer and lower tropospheric NO_x budget assessment because of the limitation of the PAN measurement discussed above, calculated losses of NO_x in this environment can be reasonably examined at all altitudes. Figures 10b and 10d show the model-predicted lifetime for NO_x as a function of altitude for the two missions. Lifetimes during March (PEM-Tropics B) are longer than September (PEM-Tropics A), particularly in the subtropics, as a direct result of the seasonality of OH. Median lifetimes range from less than a day near the surface to between 4.5 and 6.5 days in the upper troposphere.

Figure 11 shows the percentage contribution to the total NO_x destruction from the various NO_x loss pathways for tropical and subtropical regions during each campaign. In generating Figure 11, data below 4 km are limited to data points where DMS was measured in order to assess the loss pathway due to NO_3+DMS. This constraint eliminates ~40% of the data below 4 km for both missions. When DMS is measured at LOD, that value is set to zero in the model simulations to ensure that the median contributions to NO_x loss on a regional scale are not overstated.

Figure 11 shows that the formation of HNO_3 (NO_2+OH) dominates the total NO_x destruction at all altitudes, generally contributing at least half of the total destruction above 2 km, with a slight decrease in the relative contribution below 2 km. Formation of PAN as a loss of NO_x is corrected to account for the internal cycling of CH_3CO_3 and PAN as described by *Jacob et al.* [1996]. Over the subtropics during March (PEM-Tropics B), the relative contribution from HNO_3 formation is lower than that during September (PEM-Tropics A), allowing the percentage contribution from PAN formation to nearly double from 15-25% during PEM-Tropics A to 30-40% during PEM-Tropics B (Figures 11c and 11d). This difference is primarily driven by the higher concentrations of OH over the subtropics during September (PEM-Tropics A), which increases the relative rate of nitric acid formation during PEM-Tropics A by 20-30% in the

Table 2. 0-12 km Column O_3 Tendencies

	Formation $(FO_3)^a$	Destruction $(DO_3)^a$	Net Tendency $(PO_3)^a$	Reference
PEM West A (0°-18°N), (0-10 km)	1 60	2 84	-1.24	*Davis et al.* [1996]
PEM West A (18°-42°N)	3.12	3.19	-0 06	*Davis et al.* [1996]
PEM West B (0°-20°N), Low NO_x	1.61	4 02	-2.02	*Crawford et al.* [1997a]
PEM West B (0°-20°N), High NO_x	2 55	2 89	-0.35	*Crawford et al.* [1997a]
PEM West B (20°-30°N)	5.83	3.69	+2.14	*Crawford et al.* [1997b]
TRACE-A (tropical Atlantic)	11 1	10.7	+0.4	*Jacob et al* [1996]
PEM-Tropics A (0°-10°S)	1 36	3 20	-1.84	*Schultz et al.* [1999]
PEM-Tropics A (10°-30°S)	1.82	3.05	-1.23	*Schultz et al* [1999]
PEM-Tropics A (10°N-10°S)	1.43	3.14	-1.60	this study
PEM-Tropics A (10°-30°S)	1.89	3.54	-1 51	this study
PEM-Tropics B (10°N-10°S)	1 10	2.26	-1.06	this study
PEM-Tropics B (10°-30°S)	0.85	2.18	-1.21	this study

[a] 10^{11} molec cm^{-2} s^{-1}

middle and upper troposphere. Heterogeneous losses of NO_x via the N_2O_5 aerosol reaction contribute of the order of 10% to the total NO_x destruction above 8 km. Note, however, that over the subtropics during the September burning season (PEM-Tropics A), these aerosol losses remain significant down to 2 km as a result of the aerosol layers advected into the region in biomass burning plumes (Figure 11c).

The model results for PEM-Tropics A and PEM-Tropics B shown in Figure 11 indicate that the nighttime reaction of NO_3 with DMS contributes between 20-30% to the total NO_x destruction in the lowest kilometer. Over the tropical latitudes and in the boundary layer (<1 km), the median observed DMS from the DC-8 aircraft was 70 pptv during PEM-Tropics A and 89 pptv during PEM-Tropics B. Median boundary layer values were near 25 pptv for both seasons over the subtropics. Note that DMS measured from the P3-B aircraft during PEM-Tropics B was somewhat larger than the values used here from the DC-8.

The NO_3+DMS nighttime NO_x loss competes with the nighttime NO_3 and N_2O_5 loss reactions with aerosol. To determine the ultimate impact of including the NO_3+DMS reaction in models, a box model simulation was run using median observed conditions below 1 km over the PEM-Tropics A subtropics. The base simulation included the median observed DMS and the associated nighttime destruction of NO_x, while a sensitivity simulation excluded this reaction. The ultimate impact of excluding the NO_3+DMS reaction was a 25% decrease in the total NO_x destruction at 1 km and a 15% decrease at 2 km. Similar results were achieved using the data from alternate latitudes and seasons. The NO_3 and N_2O_5 nighttime loss reactions with aerosol increased only slightly in partial compensation for excluding the NO_3+DMS reaction. Thus we conclude that for remote, low NO_x, marine conditions such as found during the PEM-Tropics campaigns, the nighttime loss of NO_x to DMS in the boundary layer can be significant, contributing up to between 20 and 30% of the total NO_x loss at those altitudes.

4.4. Ozone Budget

Table 2 lists the integrated 0-12 km column O_3 tendency terms for several previous studies of tropical or subtropical areas, along with the median regional tendencies calculated in this study. All of the tropical and subtropical regions listed in Table 2 indicate either a chemical near balance or net destruction of O_3 within the 0-12 km column, with the exception of the PEM West B data from 20°-30°N, which sampled polluted Asian outflow over the northern Pacific subtropics [*Crawford et al.*, 1997b]. For the PEM-Tropics regions considered in this study (shown in Table 2), the gross formation generally equals no more than half of the gross destruction, resulting in net O_3 losses throughout the southern Pacific during both seasons. This suggests that a continual supply of O_3 into the Pacific must exist throughout the year in order to maintain O_3 levels.

The column O_3 net tendency over the tropics during PEM-Tropics B (March) is a loss of 1.06×10^{11} molecules cm^{-2} s^{-1}, increasing to a net loss of 1.60×10^{11} molecules cm^{-2} s^{-1} during PEM-Tropics A (September). Thus the seasonality inferred from these two aircraft campaigns is of the order of 50%. The net tendency at subtropical latitudes shows a similar but somewhat reduced seasonality, increasing by 25% from a net loss of 1.21×10^{11} molecules cm^{-2} s^{-1} during PEM-Tropics B (March) to 1.51×10^{11} molecules cm^{-2} s^{-1} during PEM-Tropics A (September).

Note that for PEM-Tropics A, the gross O_3 tendency terms calculated in this study agree to within better than 5% with those from *Schultz et al.* [1999], with the exception of gross destruction over the subtropics (10°-30°S) which is 15% larger in this study than that calculated by *Schultz et al.* [1999]. The latitudes used here for tropical data (10°N-10°S) encompass a larger area than that used by *Schultz et al.* [1999] (0°-10°S), but, as seen from the flight paths in Figure 1, the amount of additional data from 0° to 10°N during PEM-Tropics A is relatively small. For PEM-Tropics A, including the additional latitudes 0°-10°N changes the column O_3 net tendency by less than 1%.

4.4.1. Tropics. Figures 12a and 12b show bar plots of median gross O_3 formation and destruction terms as a function of altitude over the Tropics (10°N-10°S) for PEM-Tropics A and PEM-Tropics B. In both cases, the lower troposphere shows net destruction for O_3, while the upper troposphere shows net production, with the crossover altitude around 6 km, consistent with previous studies of remote data [e.g., *Schultz et al.*, 1999; *Davis et al.*, 1996; *Crawford et al.*, 1997b; *Jacob et al.*, 1996].

The seasonality of the integrated net O_3 tendency over the tropics was shown to be a 50% increase in the net loss from March to September (Table 2). It is apparent from Figures 12a and 12b that this seasonal difference is contained primarily within the lowest several kilometers of the troposphere and is driven by differences in the gross destruction (differences in gross formation are relatively small). For most of the extent of the tropics (east of 180° longitude), the lifetime of O_3 is similar during the two seasons. Integrated over the 0-12 km column, O_3 is destroyed in the gross sense at a rate of 6.3% d^{-1} during PEM-Tropics A and 6.4% d^{-1} during PEM-Tropics B. The variation of this destructive efficiency with altitude is likewise similar for the two seasons, as shown in Figure 12c by the asterisks (PEM-Tropics A eastern tropics) and the squares and

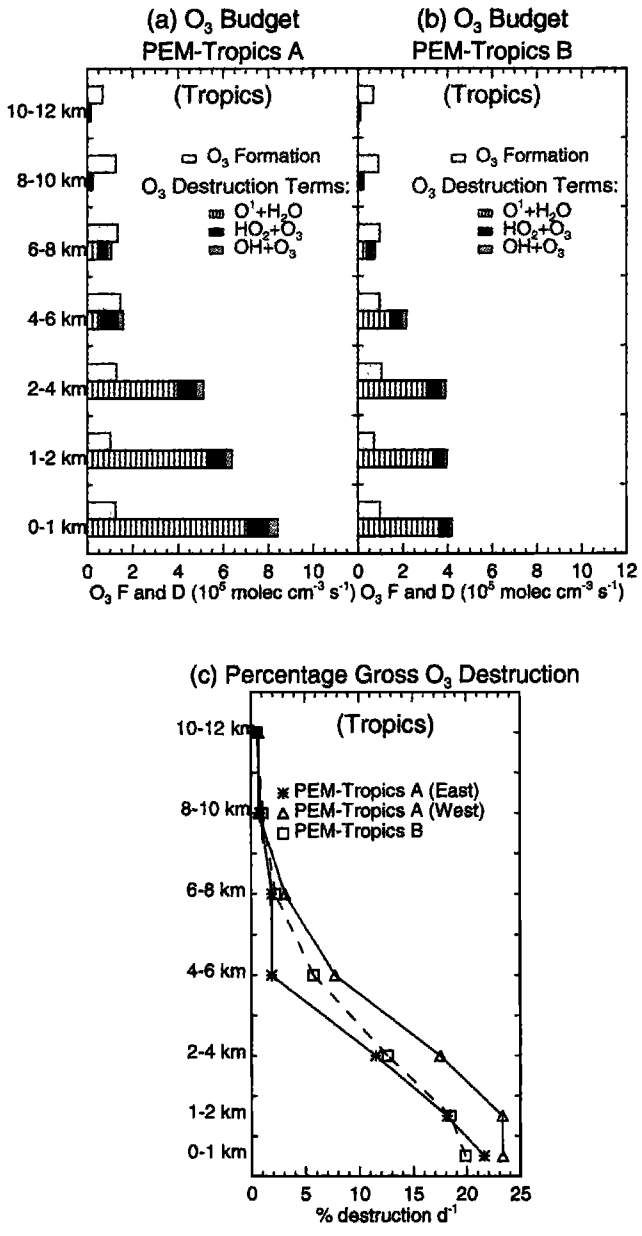

Figure 12. Photochemical O_3 budget terms over the tropics (10°N-10°S). Model-calculated, diurnal-average gross O_3 formation and destruction rates are shown for (a) PEM-Tropics A and (b) PEM-Tropics B as a function of altitude. Gross destruction is broken down into the three major components of O_3 destruction, while formation is shown as the total gross formation. (c) A vertical profile of the rate of gross O_3 destruction is shown in the form of percentage of O_3 destroyed per day during PEM-Tropics A within the tropics east of 180° (asterisks) and west of 180° (triangles) and over the tropics during PEM-Tropics B (squares and dashed line).

dashed lines (PEM-Tropics B tropics). Thus the seasonality in the net tendency over most of the extent of the tropics (east of 180°) is primarily controlled by variations in O_3. For the far western longitudes during PEM-Tropics A, where the amount of O_3 is low relative to the rest of the tropics, the seasonality remains upheld by an increase in the destructive efficiency of O_3 due to increases in lower tropospheric H_2O. This is seen in the increased destructive efficiency for the western PEM-Tropics A tropics shown in Figure 12c. Integrated over the 0-12 km column, the rate of column O_3 gross destruction is 8.3% d^{-1} at these far western longitudes.

Because water vapor is key to the rate of O_3 destruction shown here and because we found that sampling biases may impact the interpretation of tropical median values of H_2O during PEM-Tropics A (section 2.1), we examined the photochemical tendency terms in light of this potential sampling bias. When event medians are used to compute the integrated tendency terms rather than full medians, the integrated gross tendency terms are

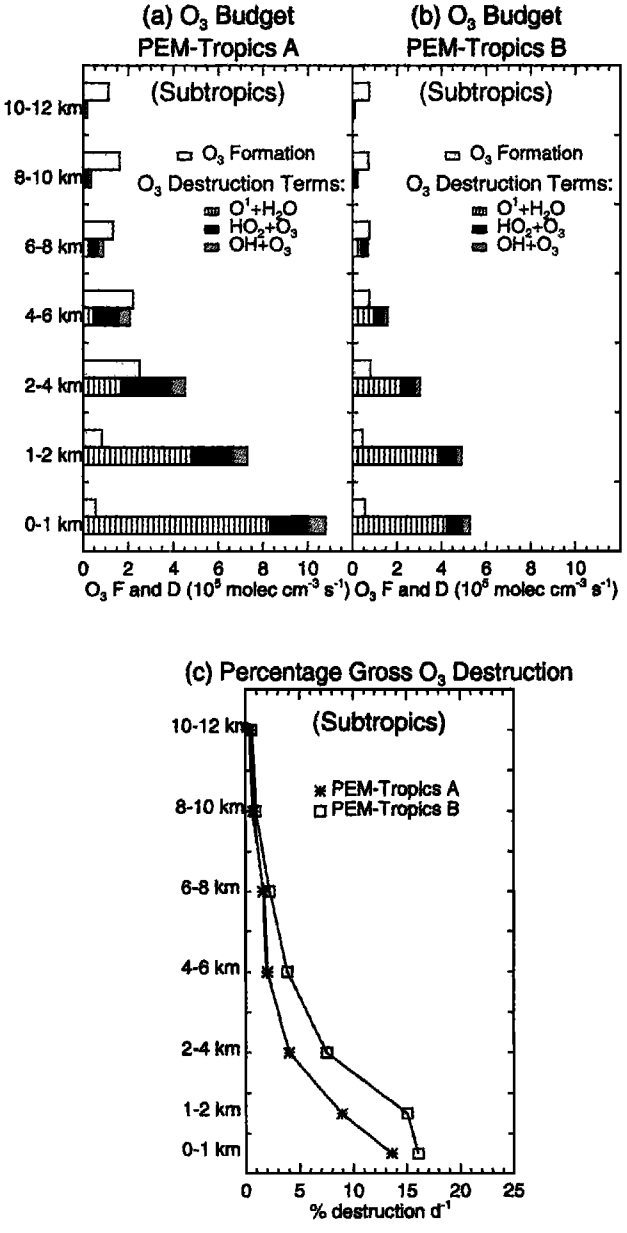

Figure 13. Photochemical O_3 budget terms over the subtropics (10°-30°S). Model-calculated, diurnal-average gross O_3 formation and destruction rates are shown for (a) PEM-Tropics A and (b) PEM-Tropics B as a function of altitude. Gross destruction and formation are as in Figure 12. (c) A vertical profile of the rate of gross O_3 destruction is shown in the form of percentage of O_3 destroyed per day within the subtropics for PEM-Tropics A (asterisks) and for PEM-Tropics B (squares).

consistent with those reported in Table 2 to within better than 10%, and the net tendency terms agree to within better than 3%.

4.4.2. Subtropics. Gross and net O_3 tendency terms for the subtropical regions shown in Table 2 indicate that while the integrated net O_3 loss is only slightly larger during PEM-Tropics A, the gross formation more than doubles while the gross destruction increases by 60%. Figures 13a and 13b show the gross O_3 formation and destruction as a function of altitude for the subtropical regions. Most of the increased gross destruction from March to September is located in the lowest several kilometers, and is consistent with the larger abundance of O_3 during PEM-Tropics A. Alternately, the increase in the gross formation is spread throughout the troposphere above the boundary layer (2 km).

Figure 13b indicates that the crossover altitude between net O_3 destruction and production lies around 6 km during PEM-Tropics B. The crossover altitude for PEM-Tropics A, however, is near 4 km (Figure 13a). Note also that during PEM-Tropics A, H_2O is the dominant destructive pathway for O_3 only in the lowest 2 km, with destruction from HO_x dominating above (Figure 13a). In contrast, PEM-Tropics B shows the loss to H_2O is dominant or equal to the loss to HO_x up to 6 km (Figure 13b). Integrated over the tropospheric column, water vapor accounts for about half of the total column O_3 destruction during PEM-Tropics A, while during PEM-Tropics B, it accounts for more than 75%.

The lifetime of O_3 is ~30% shorter during the wet season PEM-Tropics B compared to PEM-Tropics A; i.e., the percentage of the tropospheric O_3 column destroyed per day decreases from 5.5% during PEM-Tropics B to 4.0% during PEM-Tropics A. Figure 13c shows that this difference in destructive efficiency is consistent throughout the lower troposphere. The difference is largely due to the amount and distribution of water vapor. While the regional moisture conditions during the biomass burning dry season phase (PEM-Tropics A) were found to be climatologically representative by *Hu et al.* [this issue], that study shows that due to the strong La Nina signal during March 1999, conditions during PEM-Tropics B were anomalously dry relative to climatology. Thus the seasonal differences in water vapor shown by these data are probably more representative of a lower limit, as are the resulting photochemical differences.

The increased overhead column O_3 over the subtropics during PEM-Tropics A (September) is also a factor in the variance in efficiency, particularly at altitudes near the surface. Table 1 shows an increase in total overhead O_3 over the subtropics of 20 DU from PEM-Tropics B (March) to PEM-Tropics A (September). Much of this total O_3 increase is likely to be due to increases in the troposphere; the aircraft data indicate a seasonal tropospheric O_3 increase of 16 DU (see Table 1). However, photochemistry in the lowest few kilometers of the troposphere would be impacted similarly by an increased O_3 column regardless of the vertical distribution. At 20°S and at solar equinox, diurnally averaged $J(O^1D)$ at 1 km decreases by ~11% for an overhead O_3 column increase from 260 to 280 DU. The rate of O_3 destruction from the reaction H_2O+O^1D is linearly dependent on $J(O^1D)$ while HO_x concentrations, which react directly with O_3, show a sublinear dependence on $J(O^1D)$.

Thus the higher net O_3 losses during PEM-Tropics A over both the equatorial and southern subtropical Pacific are primarily driven by higher concentrations of O_3 during this time period. The seasonality in the column net loss rate is somewhat buffered over the subtropics, however. While this is partially due to the increased O_3 formation during PEM-Tropics A, the lowered seasonality is largely affected by the decreased ability of the subtropical troposphere to destroy O_3; the gross destructive efficiency is ~30% lower during PEM-Tropics A due to the drier conditions relative to PEM-Tropics B.

5. Summary

Observations of equatorial and southern subtropical trace tropospheric species during the two GTE PEM-Tropics campaigns showed distinct seasonal differences. Concentrations of O_3 and other pollutant species such as CO and NO_x were higher during PEM-Tropics A as a result of the prevalence of advection of biomass burning pollution plumes transported into the Pacific region. An exception to this is CO below 4 km in the tropical latitudes, which was larger during PEM-Tropics B and has been attributed by other studies to the low-altitude transport of northern hemispheric air into the tropical region. Additionally, water vapor during PEM-Tropics A was lower throughout the subtropics at all altitudes relative to that during PEM-Tropics B. A longitudinal gradient was evident for pollutant constituents over the tropics during PEM-Tropics A in the middle and lower troposphere, with air masses west of 180° characteristic of a clean, remote environment, and air masses east of that longitude showing influences from an anticyclonic transport of polluted subtropical air into the tropics.

A time-dependent photochemical box model was used to evaluate the photochemistry of the tropics and southern subtropics during the two campaigns. Overall, the model did a good job reproducing measured values of NO_2 and HO_x. Median NO_2 calculated-to-observed offsets were 7% during PEM-Tropics A and 3% during PEM-Tropics B. The largest underpredictions of NO_2 were at low altitudes during PEM-Tropics A and were most likely due to small offsets in the NO measurement at very low concentrations of NO (<2 pptv). The overall median calculated-to-observed ratio was 1.03 for HO_2 and 0.91 for OH, with an increased tendency toward HO_2 overprediction and OH underprediction at upper altitudes. The overprediction of upper tropospheric HO_2 is in contrast to previous model-to-measurement intercomparisons, which showed a tendency for models to underpredict HO_2 in the upper troposphere.

A steady state analysis of NO_x photochemistry indicated low values of the formation to loss ratio (F/L) in the upper troposphere, consistent with numerous previous studies; this suggests that primary NO_x sources in the upper troposphere may invalidate the steady state assumption. It is not possible to assess sources of NO_x at lower altitudes encountered during PEM-Tropics A or PEM-Tropics B due to the high percentage of time that PAN measurements were at or below the instrument LOD (1 pptv). A steady state assessment of NO_x requires a value for PAN greater than the instrument LOD, and during PEM-Tropics A and PEM-Tropics B, this subset of data represents a skewed sample of conditions when PAN has likely been transported into the boundary layer at enhanced concentrations. On the basis of the prevalence of boundary layer LOD measurements of PAN during these campaigns, we suggest that these conditions are unlikely to be typical of the remote marine environment. Throughout the region, the formation of HNO_3 dominates the NO_x loss. Within the boundary layer, the $DMS+NO_3$ nighttime reaction was found to account for up to 30% of the diurnally averaged NO_x loss at these altitudes.

The equatorial and southern subtropical Pacific region shows a significant net chemical loss for O_3 during both the

PEM-Tropics A and the PEM-Tropics B periods, implying that O_3 must be transported into the equatorial Pacific from areas outside of this geographic region throughout the year in order to maintain O_3 levels. The 0-12 km integrated net tendency showed a seasonality over the Pacific tropics, with a net loss of 1.06×10^{11} molecules cm^{-2} s^{-1} during March (PEM-Tropics B) increasing by 50% to 1.61×10^{11} molecules cm^{-2} s^{-1} during September (PEM-Tropics A). Over most of the tropics, this seasonality is primarily supported by the increased burden of O_3 during PEM-Tropics A, as O_3 lifetimes during the two seasons are similar. At the far western longitudes where O_3 concentrations were lower, the seasonal difference is supported by an increase in destructive efficiency relative to conditions during PEM-Tropics B.

The integrated column net loss for O_3 over the subtropics was calculated to be 1.21×10^{11} molecules cm^{-2} s^{-1} during March (PEM-Tropics B), increasing by 25% to a loss of 1.51×10^{11} molecules cm^{-2} s^{-1} during September (PEM-Tropics A). While the seasonality in gross destruction is supported by the increased burden of O_3 during PEM-Tropics A, it was tempered by an accompanying decrease in the destructive efficiency of the subtropical troposphere. During September (PEM-Tropics A), the tropospheric column O_3 was destroyed at the rate of 4.0% d^{-1}. This rate increased to 5.5% d^{-1} during the PEM-Tropics B season, indicating a 30% shorter O_3 lifetime during PEM-Tropics B (March).

Differences in the O_3 budget were closely tied to the seasonal variation of water vapor. According to *Hu et al.* [this issue], while the PEM-Tropics A dry season was climatologically representative, the March 1999 PEM-Tropics B wet season was anomalously dry. Therefore it can be argued that seasonal differences in the O_3 budget predicted using data from these two campaigns may be minimized.

Acknowledgments. This work was supported by the NASA Global Tropospheric Chemistry Program. The authors thank S. Madronich of the National Center for Atmospheric Research, Boulder, Colorado, for the use of the TUV Radiation Model.

References

Atkinson, R., D. L. Baulch, R. A. Cox, R. F. Hampson Jr., J. A. Kerr, and J. Troe, Evaluated kinetic and photochemical data for atmospheric chemistry, Supplement IV, IUPAC subcommittee on gas kinetic data evaluation for atmospheric chemistry, *J. Phys. Chem. Ref. Data, 21*, 1125-1568, 1992.

Avery, M. A., D. J. Westberg, H. E. Fuelberg, R. E. Newell, B. E. Anderson, S. A. Vay, G. W. Sachse, and D. R. Blake, Chemical transport across the ITCZ in the Central Pacific during an ENSO cold phase event in March/April of 1999, *J. Geophys. Res.*, this issue.

Blake, N. J., et al., Influence of southern hemispheric biomass burning on mid-tropospheric distributions of nonmethane hydrocarbons and selected halocarbons over the remote South Pacific, *J. Geophys. Res., 104*, 16,213-16,232, 1999.

Board, A. S., H. E. Fuelberg, G. L. Gregory, B. G. Heikes, M. G. Schultz, D. R. Blake, J. E. Dibb, S. T. Sandholm, and R. W. Talbot, Chemical characteristics of air from differing source regions during the Pacific Exploratory Mission -Tropics A (PEM-Tropics A), *J. Geophys. Res., 104*, 16,177-16,180, 1999.

Bradshaw, J., et al., Photofragmentation two-photon laser-induced fluorescence detection of NO_2 and NO: Comparison of measurements with model results based on airborne observations during PEM-Tropics A, *Geophys. Res. Lett., 26*, 471-474, 1999.

Brune, W. H., et al., Airborne in situ OH and HO_2 observations in the cloud-free troposphere and stratosphere during SUCCESS, *Geophys. Res. Lett., 25*, 1701-1704, 1998.

Chameides, W. L., and J. C. G. Walker, A photochemical theory of tropospheric ozone, *J. Geophys. Res., 78*, 8751-8760, 1973.

Chameides, W. L., et al., Observed and model-calculated NO_2/NO ratios in tropospheric air sampled during the NASA GTE/CITE 2 field study, *J. Geophys. Res., 95*, 10,235-10,247, 1990.

Chameides, W. L., P. Kasibhatla, and J. Yienger, Growth of continental-scale metro-agro-plexes, regional ozone pollution, and world food production, *Science, 264*, 5155-5157, 1994.

Chatfield, R., and H. Harrison, Ozone in the remote troposphere: Mixing versus photochemistry, *J. Geophys. Res.*, 81, 421-423, 1976.

Cohan, D. S., M. G. Schultz, and D. R. Blake, Convective injection and photochemical decay of peroxides in the tropical upper troposphere: Methyl iodide as a tracer of marine convection, *J. Geophys. Res., 104*, 5717-5724, 1999.

Crawford, J., et al., Photostationary state analysis of the NO_2-NO system based on airborne observations from the western and central North Pacific, *J. Geophys. Res., 101*, 2053-2072, 1996.

Crawford, J., et al., Implications of large scale shifts in tropospheric NO_x levels in the remote tropical Pacific, *J. Geophys. Res., 102*, 28,447-28,468, 1997a.

Crawford, J. H., et al., An assessment of ozone photochemistry in the extratropical western North Pacific: Impact of continental outflow during the late winter/earlier spring, *J. Geophys. Res., 102*, 28,469-28,487, 1997b.

Crawford, J., et al., Assessment of upper tropospheric HO_x sources over the tropical Pacific based on NASA GTE/PEM data: Net effect on HO_x and other photochemical parameters, *J. Geophys. Res., 104*, 16,255-16,273, 1999.

Crutzen, P. J., A discussion of the chemistry of some minor constituents of the stratosphere and troposphere, *Pure Appl. Geophys., 106-108*, 1385-1399, 1973.

Danielsen, E. F., Stratosphere-troposphere exchange based on radioactivity, ozone and potential vorticity, *J. Atmos. Sci., 25*, 502-518, 1968.

Davis, D. D., Project Gametag: An Overview, *J. Geophys. Res., 85*, 7285-7202, 1980.

Davis, D.D , et al., Photostationary state analysis of the NO_2-NO system based on airborne observations from the subtropical/tropical North and South Atlantic, *J. Geophys. Res., 98*, 23501-23523, 1993

Davis, D.D., et al., Assessment of the ozone photochemistry tendency in the western North Pacific as inferred from PEM-West A observations during the fall of 1991, *J. Geophys. Res., 101*, 2111-2134, 1996.

DeMore, W. B., S. P. Sander, D. M. Golden, R. F. Hampson, M.J. Kurylo, C. J. Howard, A. R. Ravishankara, C. E. Kolb, and M. J. Molina, Chemical kinetics and photochemical data for use in stratospheric modeling, *JPL Publ., 97-4*, 1997.

Dibb, J. E., R. W. Talbot, L. D. Meeker, E. M. Scheuer, N. J. Blake, D. R. Blake, G. L. Gregory, and G. W. Sachse, Constraints on the age and dilution of Pacific Exploratory Mission-Tropics biomass burning plumes from the natural radionuclide tracer ^{210}Pb, *J. Geophys. Res., 104*, 16,233-16,242, 1999.

Emmons, L. K., D. A. Hauglustaine, J.-F. Müller, M. A. Carroll, G. P. Brasseur, D. Brunner, J. Staehelin, V. Thouret, and A. Marenco, Data composites of airborne observations of tropospheric ozone and its precursors, *J. Geophys. Res., 105*, 20,497-20,538, 2000.

Fabian, P., and P. G. Pruchniewicz, Meridional distribution of ozone in the troposphere and its seasonal variation, *J. Geophys. Res., 82*, 2063-2073, 1977.

Faloona, I., D. Tan, and H. Fuelberg, Observations of HO_x and its relationship with NO_x in the upper troposphere during SONEX, *J. Geophys. Res., 105*, 3771-3784, 2000.

Fenn, M. A., et al., Ozone and aerosol distributions and air mass characteristics over the South Pacific during the burning season, *J. Geophys. Res., 104*, 16,197-16,232, 1999.

Fishman, J., and V. G. Brackett, The climatological distribution of tropospheric ozone derived from satellite measurements using version 7 Total Ozone Mapping Spectrometer and Stratospheric Aerosol and Gas Experiment data sets, *J. Geophys. Res., 102*, 19,275-19,278, 1997.

Fishman, J., V. Ramanathan, P. J. Crutzen, and S. C. Liu, Tropospheric ozone and climate, *Nature, 282*, 818-820, 1979.

Fishman, J., F. M. Vukovich, and E. V. Browell, The photochemistry of synoptic-scale ozone synthesis: Implications for the global tropospheric ozone budget, *J. Atmos. Chem., 3*, 299-320, 1985.

Fishman, J., K. Fakhruzzaman, B. Cros, and D. Nganga, Identification of widespread pollution in the Southern Hemisphere deduced from satellite analysis, *Science*, *252*, 1693-1696, 1991.

Fishman, J , J. M Hoell Jr., R. J. Bendura, R. J. McNeal, and V. W. J. H Kirchhoff, NASA GTE TRACE A Experiment (September-October 1992): Overview, *J. Geophys. Res.*, *101*, 23,865-23,880, 1996.

Fuelberg, H. E., R. E Newell, S. P. Longmore, Y. Zhu, D. J. Westberg, E V. Browell, D. R. Blake, G L. Gregory, and G. W. Sachse, A meteorological overview of the Pacific Exploratory Mission (PEM) Tropics period, *J. Geophys. Res.*, *104*, 5585-5622, 1999.

Fuelberg, H. E., R. E. Newell, D. J. Westberg, J. C. Maloney, J. R. Hannan, B. D. Martin, M. A. Avery, and Y. Zhu, A meteorological overview of the second Pacific Exploratory Mission in the tropics, *J. Geophys Res.*, this issue.

Gidel, L. T., and M Shapiro, General circulation model estimates of the net vertical flux of ozone in the lower stratosphere and the implications for the tropospheric ozone budget, *J. Geophys Res.*, *85*, 4049-4085, 1980.

Gregory, G. G., et al., Air chemistry over the tropical forest of Guyana, *J. Geophys. Res.*, *91*, 8603-8612, 1986.

Gregory, G G., et al., Chemical characteristic of Pacific tropospheric air in the region of the Intertropical Convergence Zone and South Pacific Convergence Zone, *J. Geophys. Res.*, *104*, 5677-5696, 1999.

Hameed, S., O. G. Paidoussis, and R. W. Stewart, Implications of natural sources for the latitude gradient of NO_y in the unpolluted troposphere, *Geophys. Res. Lett.*, *8*, 591-594, 1981.

Harriss, R.C., et al., The Amazon Boundary Layer Experiment (ABLE 2A): Dry season 1985, *J. Geophys. Res.*, *93*, 1351-1360, 1988.

Harriss, R. C., et al., The Amazon Boundary Layer Experiment: Wet season 1987, *J. Geophys. Res.*, *95*, 16721-16736, 1990.

Hoell, J. M., D. D. Davis, S. C. Liu, R. E Newell, H. Akimoto, R. J. McNeal, and R. J. Bendura, Pacific Exploratory Mission-West B (PEM-West B). February-March 1994, *J. Geophys. Res.*, *102*, 28,223-28,239, 1997.

Hoell, J. M , D. D. Davis, D. J. Jacob, M. O. Rodgers, R. E. Newell, H. E. Fuelberg, J. R. McNeal, J. L. Raper, and R. J. Bendura, Pacific Exploratory Mission in the tropical Pacific: PEM-Tropics A, August-September 1996, *J Geophys. Res.*, *104*, 5567-5584, 1999.

Horvath, S. M., and D. J. McKee, Acute and chronic health effects of ozone, in *Tropospheric Ozone, Human Health and Agricultural Impacts*, edited by David J. McKee, pp. 39-83, A. F. Lewis, New York, 1994.

Hu, Y., R. E. Newell, and Y. Zhu, Mean moist circulation for PEM-Tropics Missions, *J Geophys. Res.*, this issue.

Jacob, D J., et al., Origin of ozone and NO_x in the tropical troposphere: A photochemical analysis of aircraft observations over the South Atlantic basin, *J. Geophys. Res.*, *101*, 24,235-24,249, 1996.

Jaeglé, L., et al., Observed OH and HO_2 in the upper troposphere suggest a major source from convective injection of peroxides, *Geophys. Res. Lett.*, *24*, 3181-3184, 1997.

Jaeglé, L., D. J Jacob, W. H Brune, D. Tan, I. C. Faloona, A. J. Weinheimer, B. A. Ridley, T. L. Compos, and G. W. Sachse, Sources of HO_x and production of ozone in the upper troposphere over the United States, Geophys. Res. Lett., *25*, 1709-1712, 1998.

Kasibhatla, P. S., NO_y from sub-sonic aircraft emissions: A global three-dimensional model study, *Geophys. Res. Lett.*, *2*, 1707-1710, 1993.

Kasibhatla, P. S., H. Levy II, W. J. Moxim, and W. L. Chameides, The relative impact of stratospheric photochemical production on tropospheric NO_y levels, *J. Geophys. Res.*, *96*, 18,631-18,646, 1991.

Kasibhatla, P. S., H. Levy II, and W. J. Moxim, Global NO_x, HNO_3, PAN, and NO_y distributions from fossil fuel combustion emission: A model study, *J. Geophys. Res.*, *98*, 7165-7180, 1993.

Kasibhatla, P., H. Levy II, and T. B. Ryerson, Do emissions from ships have a significant impact on concentrations of nitrogen oxides in the marine boundary layer?, *Geophys. Res. Lett.*, *27*, 2229-2232, 2000.

Lelieveld, J., and F. J. Dentener, What controls tropospheric ozone?, *J. Geophys. Res.*, *105*, 3531-3551, 2000.

Levy, H., II, W. J. Moxim, and P. S. Kasibhatla, A global three-dimensional time-dependent lightning source of tropospheric NO_x, *J. Geophys. Res.*, *101*, 22,911-22,922, 1996.

Levy, H., II, W. J. Moxim, and P. S. Kasibhatla, Simulated tropospheric NO_x: Its evaluation, global distribution and individual source contributions, *J. Geophys. Res.*, *104*, 26,279-26,306, 1999.

Liu, S. C., D. Kley, M. McFarland, J. D. Mahlman, and H. Levy, II, On the origin of tropospheric ozone, *J. Geophys. Res.*, *85*, 7546-7552, 1980.

Logan, J.A., Nitrogen oxides in the troposphere: Global and regional budgets, *J. Geophys. Res.*, *88*, 10,785-10,807, 1983

Logan, J. A., Tropospheric ozone: Seasonal behavior, trends, and anthropogenic influence, *J. Geophys. Res.*, *90*, 10,463-10,482, 1985.

Logan, J. A., M. J Prather, S. C. Wofsy, and M B McElroy, Tropospheric chemistry: A global perspective, *J. Geophys. Res.*, *86*, 7210-7254, 1981.

Lurmann, F. W., A. C. Lloyd, and R. Atkinson, A chemical mechanism for use in long-range transport/acid deposition computer modeling, *J. Geophys. Res.*, *91*, 10,905-10,936, 1986.

McKeen, S. A., T. Gierczak, J. B. Burkholder, P. O. Wennberg, T. F. Hanisco, E. R. Keim, R.-S. Gao, S. C. Liu, A. R. Ravishankara, and D. W. Fahey, The photochemistry of acetone in the upper troposphere: A source of odd-hydrogen radicals, *Geophys. Res. Lett.*, *24*, 3177-3180, 1997.

Novelli, P. C., et al., An internally consistent set of globally distributed atmospheric carbon monoxide mixing ratios developed using results from an intercomparison of measurements, *J. Geophys Res.*, *103*, 19,285-19,294, 1998.

Olson, J., J Fishman, V. W. H. J. Kirchhoff, D. Nganga, and B. Cros, Analysis of the distribution of ozone over the southern Atlantic region, *J. Geophys. Res.*, *101*, 24,083-24,094, 1996.

Olson, J. R., B. A. Baum, D. R. Cahoon, and J. H. Crawford, Frequency and distribution of forest, savanna, and crop fires over tropical regions during PEM-Tropics A, *J. Geophys Res.*, *104*, 5865-5876, 1999.

Penner, J. E., C. S. Atherton, J. Dignon, S. J. Ghan, J. J. Walton, and S. Hameed, Tropospheric nitrogen: A three-dimensional study of sources, distributions, and deposition, *J. Geophys. Res.*, *96*, 959-990, 1991.

Prather, M., and D. J. Jacob, A persistent imbalance in HO_x and NO_x photochemistry of the upper troposphere driven by deep tropical convection, *Geophys. Res. Lett.*, *24*, 3189-3192, 1997.

Ramanathan, V., and R. E. Dickinson, The role of stratospheric ozone in the zonal and seasonal radiation energy balance of the earth troposphere system, *J Atmos. Sci.*, *36*, 1084-1104, 1979.

Ramanathan, V., L. B. Callis, and R. W. Boughner, Sensitivity of surface temperature to perturbations in the stratospheric concentrations of ozone and nitrogen dioxide, *J. Atmos. Sci.*, *33*, 1092-1112, 1976.

Raper, J. L., M. M. Kleb, D. J. Jacob, D. D. Davis, R. E. Newell, H. E. Fuelberg, R. J. Bendura, J. M. Hoell, and R. J. McNeal, Pacific Exploratory Mission in the tropical Pacific: PEM-Tropics B, March-April 1999, *J. Geophys. Res.*, this issue.

Roelofs, G.-J., J. Lelieveld, and R. van Dorland, A three dimensional chemistry/general circulation model simulation of anthropogenically derived ozone in the troposphere and its radiative climate forcing, *J. Geophys. Res.*, *102*, 23,389-23,401, 1997.

Schultz, M. G., et al., On the origin of tropospheric ozone and NO_x over the tropical South Pacific, *J. Geophys. Res.*, *104*, 5829-5843, 1999.

Schultz, M. G., D. J. Jacob, and H. B. Singh, Chemical NO_x budget in the upper troposphere over the tropical South Pacific, *J. Geophys. Res.*, *105*, 6669-6680, 2000.

Shetter, R. E., and M. Müller, Photolysis frequency measurements using actinic flux spectroradiometry during the PEM-Tropics mission: Instrumentation description and some results, *J. Geophys. Res.*,*104*, 5647-5662, 1999.

Tan, D., et al., OH and HO_2 in the remote tropical Pacific: Results from PEM-Tropics B, *J. Geophys. Res.*, this issue.

Thompson, A. M., K. E. Pickering, D. P. McNamara, M. R. Schoeberl, R. D. Hudson, J. H. Kim, E. V. Browell, V. W. J. H. Kirchhoff, and D. Nganga, Where did tropospheric ozone over southern Africa and the tropical Atlantic come from in October 1992? Insights from TOMS, GTE TRACE A, and SAFARI 1992, *J. Geophys. Res.*, *101*, 24,251-24,278, 1996.

Wang, Y., J. A. Logan, and D. J. Jacob, Global simulation of tropospheric O_3-NO_x-hydrocarbon chemistry, 2, Model evaluation and global ozone budget, *J. Geophys. Res.*, *103*, 10,727-10,755, 1998.

Wennberg, P. O., et al., Hydrogen radicals, nitrogen radicals, and the production of O_3 in the upper troposphere, *Science*, *279*, 49-53, 1998.

M.A. Avery, J.D.W. Barrick, J.H. Crawford, J.R. Olson, G W. Sachse, and S.A. Vay, Atmospheric Sciences Competency, NASA Langley Research Center, Hampton, Virginia. (j.r.olson@larc.nasa.gov)

D.R. Blake, Department of Chemistry, University of California-Irvine, Irvine, California.

W.H. Brune and I.C. Faloona, Department of Meteorology, Pennsylvania State University, University Park, Pennsylvania.

G. Chen, D.D. Davis, S.T. Sandholm, D. Tan, School of Earth and Atmospheric Sciences, Georgia Institute of Technology, Atlanta, Georgia.

B.G. Heikes, Center of Atmospheric Chemistry Studies, Graduate School of Oceanography, University of Rhode Island, Narragansett, Rhode Island.

B.L. Lefer and R.E. Shetter, Atmospheric Chemistry Division, National Center for Atmospheric Research, Boulder, Colorado.

H.B. Singh, Chemistry and Dynamics Branch, NASA Ames Research Center, Moffett Field, California.

R.W. Talbot, CSRC/EOS, University of New Hampshire, Durham, New Hampshire.

(Received October 3, 2000; revised January 19, 2001;
accepted January 24, 2001.)